Title Page

Full title: Molecular characterization of nervous system organization in the hemichordate *Saccoglossus kowalevskii*

Short title: Nervous system organization in a hemichordate

Author List

José M. Andrade Lopéz, Ariel M. Pani, Mike Wu, John Gerhart, Christopher J. Lowe*

Author affiliation

1) Hopkins Marine Station, Department of Biology, Stanford University, 120 Oceanview Blvd., Pacific Grove, CA 93950, United States

2) Departments of Biology and Cell Biology, University of Virginia, 90 Geldard Drive, Charlottesville, VA 22903

3) Department of Molecular and Cell Biology, University of California, 142 Life Sciences Addition #3200, Berkeley, CA 94720-3200

* corresponding author

Abstract

Hemichordates are an important group for investigating the evolution of bilaterian nervous systems. As the closest chordate outgroup with a bilaterally symmetric adult body plan, hemichordates are particularly informative for exploring the origins of chordates. Despite the importance of hemichordate neuroanatomy for testing hypotheses on deuterostome and chordate evolution, adult hemichordate nervous systems have

not been comprehensively described using molecular techniques, and classic histological descriptions disagree on basic aspects of nervous system organization. A molecular description of hemichordate nervous system organization is important for both anatomical comparisons across phyla and for attempts to understand how conserved gene regulatory programs for ectodermal patterning relate to morphological evolution in deep time. Here, we describe the basic organization of the adult hemichordate *Saccoglossus kowalevskii* nervous system using immunofluorescence, *in situ* hybridization, and transgenic reporters to visualize neurons, neuropil, and key neuronal cell types. Consistent with previous descriptions, we found the *S. kowalevskii* nervous system consists of a pervasive nerve plexus that is concentrated in the anterior, along with nerve cords on both the dorsal and ventral sides. Neuronal cell types exhibited clear anteroposterior and dorsoventral regionalization in multiple areas of the body. We observed spatially demarcated expression patterns for many genes involved in synthesis or transport of neurotransmitters and neuropeptides but did not observe clear distinctions between putatively centralized and decentralized portions of the nervous system. In the trunk, there is a clear division of cell types between the dorsal and ventral cords suggesting differences in function. The plexus shows regionalized structure and is consistent with the proboscis base as a major site for information processing rather than the dorsal nerve cord. The absence of neural processes crossing the basement membrane into muscle and extensive axonal varicosities suggest that volumetric transmission may play an important role in neural function. These data now facilitate more informed neural comparisons between hemichordates and other groups and contribute to broader debates on the origins and evolution of bilaterian nervous systems.

Introduction

The evolution and origins of animal nervous systems has been a topic of debate in comparative literature for over a century, and the origins of the chordate nervous system has been a topic of particular interest (Bateson, 1886; Garstang, 1894; Garstang, 1928; Geoffroy-St. Hilaire, 1822). With the emergence of

molecular genetic data, the origins of brains and the deep ancestry of central nervous systems (CNS) has been a fascination in the field of evolution of development (Arendt and Nubler-Jung, 1996; De Robertis and Sasai, 1996; Denes et al., 2007; Hirth, 2010; Holland, 2015; Lowe et al., 2003; Martin-Duran et al., 2018). Classical comparative neurobiology has a rich and long history with broad phylogenetic sampling that was instrumental in developing many of the major hypotheses in neurobiology and nervous system evolution (Bullock and Horridge, 1965). The spectacular innovations in molecular neuroscience have given unprecedented insights into neural function (Luo, 2020). However, the focus of this work has been largely on biological models with highly centralized nervous systems and strong cephalization, particularly arthropods and vertebrates (Hejnol and Lowe, 2015). There have been fewer comprehensive molecular studies in phyla outside of these clades, particularly in animals with more sedentary lifestyles and less obvious centralization. Yet, for a broader understanding of nervous system evolution in metazoans, contemporary molecular data from these phyla is essential. This is now particularly pressing, as the generation of comparative developmental patterning data of regulatory genes, with key roles in CNS specification and patterning of arthropods and vertebrates, has now been investigated quite broadly phylogenetically, and by far outpaced parallel contemporary characterizations of neural cell type identity, and nervous system structure and function in the same representative species. Application of modern molecular tools of neurobiology to a wider range of species representing a broader sampling of neural systems is now essential, and not only test prevailing views on the evolution of the nervous system, but also provide novel opportunities to investigate neural circuit evolution.

Hemichordates are a group of marine invertebrates with sedentary adult life histories that have long been of comparative interest particularly in relation to chordate evolution (Kaul-Strehlow and Röttinger, 2015; Lowe, 2021; Tassia et al., 2016). Hemichordates were originally grouped within chordates due to proposed morphological affinities with chordates (Bateson, 1885). A close phylogenetic relationship with echinoderms based on larval morphology were recognized as early as the late 1800s (Metschnikoff, 1881), and all molecular studies have robustly grouped hemichordates as the sister group of echinoderms

within the deuterostomes (Bromham and Degnan, 1999; Cameron et al., 2000; Cannon et al., 2014; Furlong and Holland, 2002). Hemichordates are divided into two major lineages; Enteropneusta and Pterobranchia. Enteropneusta are free-living worms that mainly live in burrows feeding by filter feeding or by particle ingestion, whereas Pterobranchs are small, largely colonial animals that have received far less research attention, due to their scarcity and small size (Sato et al., 2008; Tassia et al., 2016).

The earliest descriptions of the nervous system of enteropneusts using classical staining methods began in the late 1800s (Bateson, 1886; Kowalevsky, 1866; Spengel, 1877, 1903) and continued sporadically in the early to mid 1900s (Bullock, 1940, 1944; Bullock, 1945; Dawydoff, 1948; Hess, 1937; Knight-Jones, 1952). Only a few studies have used electron microscopy for more detailed structural observations (Dilly, 1969; Dilly et al., 1970; Kaul and Stach, 2010; Kaul-Strehlow and Stach, 2013). The enteropneust nervous system is largely intraepidermal with a basiepithelial plexus throughout the animal, but more prominent anteriorly in the proboscis and collar, and thickest at the base of the proboscis and proboscis stem (Fig 1). There are two cords, one ventral that is basiepidermal, extending from the posterior collar to the posterior of the trunk, and dorsal cord that extends along the entire extent of the dorsal midline. From the anus to the collar, this dorsal cord is superficial and basiepidermal, but the cord is internalized in the collar into a subepidermal cord, which in some species resembles vertebrate neural tube (Bateson, 1886; Kaul and Stach, 2010; Luttrell et al., 2012). At its most anterior extent, the collar cord emerges at the proboscis stem and continues as a superficial cord along the length of the proboscis. The two cords are connected by a nerve ring in the posterior collar. Classical studies of hemichordate enteropneust nervous systems have come to contrasting conclusions on the most basic organizational principles of their structure and function. Some studies focused on the importance of the two cords, dorsal and ventral, acting as potential integration centers and concluded that hemichordates possess a CNS (Bateson, 1886; Hess, 1937; Morgan, 1894), whereas others have focused on the broadly distributed epithelial plexus with dorsal and ventral cords acting as conduction tracts instead of integration centers (Bullock, 1940; Bullock, 1945; Knight-Jones, 1952). From work in separate species, Bateson and Morgan concluded that the

enteropneust collar cord, an intraepidermal cord, was homologous to the dorsal cord of chordates (Bateson, 1886; Morgan, 1894) because of the striking similarities to the subepidermal hollow cord, that in some species forms by a morphological process that strongly resembles vertebrate neurulation. Later studies in the 1930s-50s hypothesize that the dorsal and ventral cord were conduction tracts that lack neural cell bodies (Bullock 1945, Knight-Jones 1952). Bullock believed that the hemichordate nervous system more closely resembled the nerve net of cnidarians (Bullock 1945) whereas Knight-Jones alternatively proposed that the collar cord may be homologous to the neural tube in chordates but had since been secondarily simplified and is now largely a through tract rather than an integrative center (Knight-Jones 1952). More recent studies based on comparative morphology have added support to the hypothesis of homology between the hemichordate collar cord and the chordate dorsal cord (Kaul and Stach, 2010; Luttrell et al., 2012)

Recent interest in bilaterian neural system evolution has been driven by body patterning comparisons and the remarkable similarities between the development of central nervous systems of distantly related nervous systems (Arendt and Nubler-Jung, 1994; De Robertis, 2008; De Robertis and Sasai, 1996; Hirth, 2010; Hirth and Reichert, 1999; Lichtneckert and Reichert, 2005). Most molecular insights into hemichordate neural development have been inferential, using patterning genes rather than genes with roles in neural cell type differentiation (Aronowicz and Lowe, 2006; Darras et al., 2018; Gonzalez et al., 2017; Lowe et al., 2006; Lowe et al., 2003; Pani et al., 2012; Yao et al., 2016). However, some studies have focused specifically on genes with established roles in neural specification and differentiation, or cross-reactive antibodies for neural epitopes (Cunningham and Casey, 2014; Kaul-Strehlow et al., 2015; Lowe et al., 2003; Miyamoto et al., 2010; Nomaksteinsky et al., 2009). These studies have used pan-neural markers, like *elav* and synaptotagmin, and enzymes involved in neurotransmitter synthesis to study the hemichordate nervous system. Although limited, these studies have continued to show evidence of a broad plexus, but again have come to contrasting conclusions about the nature of the enteropneust nervous system. There is still no comprehensive study of neural subtypes and their distribution in

125 hemichordates, nor a clear picture of the morphology for different cell types or structure of the neural
126 plexus and cords.
127
128 Speculation on the organization of the enteropneust nervous system was reignited with the studies on the
129 expression of gene regulatory networks (GRN) with conserved roles in patterning the CNS of many
130 model species during the early development of *S. kowalevskii*. The GRN for anterior-posterior CNS
131 patterning that is well conserved between several protostomes groups and chordates is also conserved in
132 hemichordates along the anterior-posterior (AP) axis even though the nervous systems they specify are
133 anatomically very different (Darras et al., 2018; Gonzalez et al., 2017; Kaul-Strehlow et al., 2017; Lowe
134 et al., 2003; Pani et al., 2012; Yao et al., 2016). These genes are expressed in circular bands around the
135 ectoderm in hemichordates, rather than expressed in a tight domain associated with either the dorsal or
136 ventral cords, unlike in vertebrates where they are most prominently expressed in the developing brain
137 and nerve cord (Pani et al., 2012). The neural structures specified by this conserved network have evolved
138 independently and represent highly divergent structures despite the tight conservation in their gene
139 regulatory networks. Therefore, it remains an open question as to whether there are some elements of
140 neural conservation despite the overt differences in the organizational elements of their respective
141 nervous systems. It also remains a possibility that there are neural cell type homologies under conserved
142 positional regulation between vertebrates and hemichordates. A closer examination of the molecular
143 neurobiology of hemichordates and the potential link to conserved suites of regulatory genes will
144 contribute to the discussion about how molecular genetic data can be used to reconstruct ancestral neural
145 architectures.
146
147 Here we characterize the expression of multiple neural markers using *in situ* hybridization, and
148 immunohistochemistry to characterize the location and degree of specialization of the nervous system
149 along both the AP and dorsal-ventral (DV) axes, and the extent and structure of the neural plexus. We
150 also used mosaic transgenic approaches to determine cellular morphologies and projection patterns of

151 neural subpopulations. Our data provides the first comprehensive description, to our knowledge, of an
152 adult hemichordate nervous system using molecular methods, which will facilitate comparisons to other
153 bilaterians.
154

155 ## Results

156

157 **Extent and regionalization of neural markers along the A/P and D/V axes**

158 Many classical studies of enteropneust nervous systems used histological techniques, such as Golgi stains,
159 that generally work well in animals with a clearly defined CNS where neurons are segregated from the
160 general epithelium. However, these methods may not unambiguously distinguish neural from epidermal
161 cells in animals, like enteropneusts, where the nervous system is intraepidermal. Consequently, the
162 number, diversity, and distribution of neurons along the A/P and D/V axes of the adult animals has been a
163 source of controversy (Bullock, 1945). We examined expression of a wide range of neural/neurosecretory
164 markers in post-hatching juvenile and fully grown adult animals, using *in situ* hybridization. Previous
165 studies have demonstrated that neurons are specified across broad domains during embryogenesis, and
166 nerve cords are first apparent during late stages of embryonic development (Cunningham and Casey,
167 2014; Kaul-Strehlow et al., 2015). Our study focused on post-hatching juveniles as the animal possesses
168 almost all the adult characteristics but are smaller and more amenable to whole-mount microscopy. This
169 initial part of our study establishes a more accurate assessment of neural cell body number, the extent of
170 neural subtypes, and how they are distributed along the major organizational axes.
171

172 ***Elav* expression in the *S. kowalevskii* nervous system:** *Embryonic lethal abnormal visual system (elav*)
173 is a conserved RNA binding protein, first discovered in *Drosophila melanogaster* that has been used in

174 many organisms as a putative pan-neuronal marker (Cunningham and Casey, 2014; Robinow et al., 1988;
175 Robinow and White, 1988). However, expression of *elav* has been reported in other cell types, and does
176 not always mark the entire neural complement (Pham and Hobert, 2019; Sanfilippo et al., 2016), so
177 caution should be used when only using this marker to fully represent neural complements in developing
178 models. We first sought to identify the distribution of *elav*+ cells in juveniles and adult tissue by *in situ*
179 hybridization, extending the scope of previous studies at earlier developmental stages (Cunningham and
180 Casey, 2014; Lowe et al., 2003). This gene has previously been shown to exhibit a tight association with
181 the forming cords on the trunk midlines and expressed broadly in the proboscis ectoderm (Cunningham
182 and Casey, 2014; Lowe et al., 2003; Nomaksteinsky et al., 2009), but with few cells outside of the cords,
183 posterior to the collar.
184
185 We first examined *elav* expression in adult *S. kowalevskii* through a comprehensive series of adult
186 sections in both transverse and sagittal planes (Fig 1A). The transverse plane at mid-proboscis shows
187 circumferential *elav* expression in the most basal layer of the epithelium, and more marked staining along
188 the dorsal midline (Fig 1B). The cross section at the proboscis base has a thicker band of expression,
189 supporting previous observations of neural condensation in this region (Nomaksteinsky et al., 2009) (Fig
190 1C). At the anterior collar, we detected expression of *elav* throughout the pharyngeal epithelium (Fig 1D-
191 G) and evidence of the anterior collar nerve ring in the ectoderm (Fig 1D). In addition, there is a
192 prominent layer of *elav* expression dorsal to processes in the dorsal cord, representing the soma of that
193 runs the length of the collar as an internal collar cord (Fig 1D-I). Expression in the general ectoderm of
194 collar and trunk is sparse, as described previously in *Ptychodera flava* (Nomaksteinsky et al., 2009) but
195 cells are detected in the epithelium in the posterior collar and trunk (Fig 1H-J). Sagittal sections show a
196 gradient of *elav* expression in the proboscis increasing towards the base, an anterior collar ring (ACR) and
197 posterior collar ring, and expression in the pharyngeal endoderm (Fig 1K,L,M). The middle sagittal
198 section clearly shows the trajectory of the collar cord (Fig 1L). The enteric nervous system is also visible
199 in the endoderm with dispersed *elav*+ cells in the gut (Fig 1M). At late juvenile stage, characterized by

200 the presence of 3-gill slits (3GS), *elav*+ cells are distributed similarly to their distribution in adults;
201 throughout the proboscis ectoderm, with a concentration at the proboscis base, and also along the entire
202 dorsal and ventral cords (Fig 1N). The proboscis dorsal cord is also visible and extends anteriorly from
203 the collar cord (Fig 1O). The similarities between adult and late juvenile suggests that the juvenile is a
204 reasonable approximation for basic organization of adult neural characters.
205
206 Given the comparative interest in hemichordate trunk nerve cords and distribution of neurons in the skin,
207 we examined *elav* expression closely in adults using whole mount *in situ* hybridization to visualize cell
208 populations that may be difficult to observe in tissue sections. In the ventral cord, expression of *elav* is
209 broadly expressed in a wide band of ectoderm. Rows of clustered cells are present in columns,
210 perpendicular to the cord, along ridges of the epithelium (Fig 1P). On the dorsal side, a thin line of *elav*+
211 cells is present along the length of the proboscis (Fig 1Q), along with the broad expression shown in
212 sections (Fig 1B,C). Expression is also detected in two narrow rows of cells that flank the dorsal midline
213 along the length of the trunk (Fig 1R,S). In the trunk, the *elav*+ domain is markedly narrower on the
214 dorsal side than the ventral side. In the posterior trunk, *elav*+ cells are also distributed in clusters of cells
215 throughout the epithelium, possibly associated with the calcified granules embedded in this region (Fig
216 1S).
217

218 **Regionalization of neural subtypes**

219

220 **Expression of neurotransmitter and neuropeptide biosynthesis and transport markers:** While
221 general neural markers like *elav* give a broad picture of the localization of neurons, they do not give any
222 insights into the extent of neural diversity, or how neural subpopulations are organized. Expression of
223 genes involved in the biosynthesis and transport of neurotransmitters and neuropeptides provides
224 information about the extent of neural differentiation, and how organized their expression domains are

225 along organizational axes. We performed *in situ* hybridization for components of neurotransmitter and
226 neuropeptide signaling, including proteins involved in their synthesis and transport in juvenile, both at the
227 1 gill-slit (1GS) and 3GS stage, and in some cases, in adult tissue.
228
229 Neurotransmitters are small molecules used by neurons as chemical messengers to communicate across
230 cells. They can transmit an excitatory or inhibitory signal synaptically, or modulate neuronal activity non-
231 synaptically using biogenic amines (or monoamines) and amino acids. Genes involved in neurotransmitter
232 synthesis and transport are often highly regionalized in the nervous systems of model bilaterian species.
233
234 **Monoamine neurotransmitters**: In *Saccoglossus* juveniles, the location of catecholaminergic neurons is
235 revealed by the expression of *tyrosine hydroxylase* (*TH*) in scattered cells at several different domains in
236 the ectoderm. Early developmental stages were examined previously (Cunningham and Casey, 2014). In
237 early juveniles, shortly after hatching *TH* expression is restricted to isolated cells in the anterior proboscis
238 ectoderm, and broadly in the anterior trunk, wrapping around the forming first gill slit (Cunningham and
239 Casey, 2014; Pani et al., 2012). This pattern continues in the later juvenile stages before hatching with the
240 addition of a thin circumferential line close to the base of the proboscis (Fig 2A). The expression around
241 the gill slits is far more diffuse and extensive than the more cell type specific staining in the proboscis and
242 collar (Fig 2A,A',C). In post hatching juveniles, an additional prominent band of cells forms at the
243 anterior tip of the collar (Fig 2A'). The same general expression domains persist through to adults, but
244 with an expanded anterior proboscis domain (Fig 2B), and additional isolated cells in the collar, with a
245 strong anterior collar domain, and row of cells at the base of the proboscis (Fig 2B'). To specifically
246 identify dopaminergic neurons, we examined the expression of *dopamine transporter* (*DAT*). In juveniles,
247 *DAT* is co-expressed in many of the same cells in the juveniles (Fig 2C); in the anterior proboscis (Fig
248 2C') and in anterior collar (Fig 2C''). *TH*+ cells at the base of the proboscis were conspicuously missing
249 *DAT* co-expression, raising the possibility they may represent other types of catecholaminergic neurons.

250 However, in older juveniles, *DAT* is expressed in this region and supports the DA neural identity (Fig
251 2C''').
252
253 The distribution of *tryptophan hydroxylase* (*TPH*), marking serotonergic neurons, was previously
254 reported at earlier developmental stages (Cunningham and Casey, 2014). Here we confirm isolated
255 cellular expression in a broad circumferential domain in the proboscis ectoderm shortly after hatching
256 (Fig 2D). Histamine is synthesized from histidine by *histidine decarboxylase* (*HDC*) and is a marker for
257 histaminergic neurons (Watanabe et al., 1984). In juveniles, expression of *HDC* is sharply defined in the
258 posterior proboscis in a broad ectodermal domain rather than punctate individual cells, which may
259 indicate a broader ectodermal distribution of histamine rather than specifically neuronal (Fig 2E).
260 Additionally, more punctate staining is detected in the ventral ectoderm narrowing to the ventral cord at
261 later stages, and scattered large cells along the dorsal cord in the trunk, which refine to a more posterior
262 territory at later stages (Fig 2E,E').
263
264 **Amino acid neurotransmitters:** Two major amino acid neurotransmitters are glutamate and GABA.
265 Glutamate is a major excitatory neurotransmitter across bilaterians and non-bilaterians (Antzoulatos and
266 Byrne, 2004; Danbolt, 2001; Fonnum, 1984; Greer et al., 2017; Nistri and Constanti, 1979). GABA has a
267 conserved role in bilaterians as an inhibitory neurotransmitter in both the CNS and PNS in invertebrates
268 and vertebrates (Gerschenfeld, 1973; Jackson et al., 1990; McIntire et al., 1993; Miller, 2019; Mueller et
269 al., 2006; Nistri and Constanti, 1979; Roberts et al., 1976). Expression of *glutamate decarboxylase* (*GAD*)
270 has been used to characterize the distribution of GABA–producing neurons (Roberts and Kuriyama,
271 1968) along with the GABA transporter *VGAT* (Kinjo et al., 2013), whereas glutamatergic neurons have
272 been identified by the expression of its transporter, *VGluT*.
273
274 In *Saccoglossus* juveniles, *VGluT* is detected in isolated cells in the ectoderm of the proboscis and
275 anterior collar (Fig 2F). In the trunk, it is detected in two rows of cells on either side of the dorsal midline

276 along the trunk, posterior to the collar (Fig 2F, inset) at early juvenile stage and in scattered cells broadly
277 in the posterior. In 3GS juveniles, expression in the proboscis remains broadly dispersed, and there are
278 two circumferential lines of cells in both the anterior and posterior collar (Fig 2F'). Expression extends
279 down the trunk, again along the dorsal midline in a broad territory, wider than the extent of the cord
280 defined by the expression of *elav* (Fig1N,O,R), but also dispersed in the general ectoderm (Fig 2F'').
281 *GAD* is expressed in scattered ectodermal cells in defined domains throughout different developmental
282 stages. In early juveniles it is expressed throughout the entire proboscis, but most prominently in the
283 anterior tip and at the proboscis base (Fig 2G). At later juvenile stages, the anterior and posterior
284 ectodermal, circumferential domains become more prominent, and a sharp, narrow band of expression at
285 the very anterior lip of the collar is detected in a circumferential domain. At these later stages, expression
286 is now detected in isolated cells in the posterior region of the pharynx and in scattered cells in the dorsal
287 cord of the trunk (Fig 2G'). The juvenile expression is consistent with the patterns found in adult animals:
288 the whole mount *in situ* hybridization of adult *GAD* expression reveals a dense anterior expression
289 domain that becomes increasingly diffuse down towards the proboscis base (Fig 2H). There is a
290 pronounced ring of cells at the proboscis base that is contiguous except dorsally where the ring terminates
291 with a pair of prominent cell clusters on either side of the dorsal midline (Fig 2H'). The anterior lip of the
292 collar has a similar ring in isolated cells (Fig 2H'). The distribution of the GABA transporter *VGAT* in
293 early juveniles shows very similar expression domains to *GAD* at early juvenile stages, with strong
294 expression at the base of the proboscis and cells scattered throughout the ectoderm (Fig 2I,I'). However,
295 we do not observe expression in the anterior proboscis where *GAD* is localized at either early or late
296 juvenile stage.
297

298 **Neuropeptides**: Neuropeptides are the largest and most diverse signaling molecules ranging from 3-40+
299 amino acids that are involved in neurotransmission, neuromodulation or hormonal functions (Burbach,
300 2011; van den Pol, 2012). Most neuropeptides signal through G protein-coupled receptors (GPCRs) to

301 modulate downstream activities (Hewes and Taghert, 2001; Jekely, 2013). Previous studies have
302 identified an array of conserved neuropeptides and their GPCR receptors in *S. kowalevskii* (Elphick, 2010;
303 Elphick and Mirabeau, 2014; Jekely, 2013; Krishnan et al., 2013; Mirabeau and Joly, 2013). Three
304 general neuropeptide synthesis enzymes are Prohormone convertase 2 (PC2), glutaminyl-peptide
305 cyclotransferase (GPC), and peptidyl glycine α-amidating monooxygenase (PAM), which catalyzes the
306 posttranslational modification of the N-terminal glutamine (GPC) or the C-terminal glycine (PAM) of
307 peptide hormones (Busby et al., 1987; Fischer and Spiess, 1987; Rouille et al., 1995; Seidah et al., 1999;
308 Zhang et al., 2010). Expression of these markers reveals the general regional expression of the diverse
309 array of neuropeptides in *S. kowalevskii.* Expression of these enzymes exhibit generally overlapping
310 localization in both early and late juveniles (Fig 3A-B), with many cells co-expressing multiple
311 neuropeptide synthesis markers (Fig 3C-C'''). In early juveniles, PC2 is broadly expressed in the
312 proboscis, but strongest at the base (Fig 3D). It has a tight ring of expression in the anterior collar, in the
313 collar/dorsal cord, and in the developing ventral cord (Fig 3D). Expression in the later juvenile is
314 strongest at the base of the proboscis, anterior collar ring, and anterior ventral cord, whereas expression in
315 the anterior proboscis and dorsal cord becomes less prominent (Fig 3D'). GPC expression is more
316 dorsally localized at the proboscis base with more punctate expression in the ventral ectoderm (Fig 3E,E')
317 whereas PC2 expression is more uniform in a thick band around at the proboscis base (Fig 3D,D'). We
318 also observed expression in the more posterior regions of the dorsal and ventral cords. Together, these
319 enzymes are expressed at the five major regions of the ectoderm: anterior proboscis, posterior proboscis,
320 anterior collar, dorsal cord, and the ventral cord and overlap in their expression domains in the proboscis
321 and collar with several of the neurotransmitter systems.

322

323 A wide range of neuropeptides have been identified in *S. kowalevskii* (Elphick, 2010; Elphick and
324 Mirabeau, 2014; Jekely, 2013; Krishnan et al., 2013; Mirabeau and Joly, 2013), and we investigated the
325 expression of a small subset of these. A major group of diverse neuropeptides have a typical c-terminal

326 signature, many of which are phyla-specific, including the RFamides, which have the conserved c-
327 terminal RFamide amino acid sequence. There are hundreds of RFamides that have been described across
328 bilaterians, and each is involved in diverse roles ranging from osmoregulation, muscle contractions,
329 reproduction, feeding and digestion (Elphick and Mirabeau, 2014; Jekely, 2013; Mirabeau and Joly, 2013;
330 Walker et al., 2009). The original RFamide, FRMRamide, was identified from the ganglia of a mollusk,
331 *Macrocallista nimbosa*, and was later characterized for its role as a caridioexcitatory neuropeptide (Price
332 & Greenberg 1977).
333
334 *S. kowalevskii* contains many of these neuropeptides with a signature c-terminal sequence including
335 VIamide, Luqin (RWamide), WFMRFamide, and NNFamide. VIamide is characterized by an anterior,
336 dorsal domain of expression in early and late juveniles, with isolated cells along the dorsal midline from
337 the anterior tip to about half way down the proboscis (Fig 3G,G'). The conserved bilaterian neuropeptide
338 luqin (Luq), subsequently lost in the chordate lineage (Elphick and Mirabeau, 2014), is an RFamide-
339 related neuropeptide. Comparative studies across bilaterians suggest a shared role in chemosensory and
340 locomotion control through flask shaped, ciliated RFamide neurons (Tessmar-Raible et al., 2007). Luq is
341 initially expressed in the posterior proboscis and anterior collar at the 1GS stage but expression is later
342 detected at the anterior and posterior proboscis, anterior collar, both the dorsal and ventral cord, and the
343 ventral cord extends towards the post anal tail in 3GS juveniles (Fig 3H,H'). WFMRFamide expression
344 appears as scattered cells in the anterior proboscis and strong circular bands at the proboscis base and
345 anterior collar in both early and late juveniles (Fig 3J,J'). Expression also appears in the trunk around the
346 gill slits and ciliary band in late juveniles (Fig 3J'). NNFamide is expressed in the proboscis ectoderm in
347 two main domains; the most prominent is in a strong, circumferential, horseshoe-shaped band with
348 expression absent in the most dorsal territory, close to the base of the proboscis (Fig 3K,K'). The second
349 domain is defined by scattered individual cells visible in the entire anterior half of the proboscis
350 ectoderm, all the way to the anterior tip.

351

352 The hypothalamic-pituitary axis (HPA) is a major neuroendocrine system associated with the regulation
353 of many biological and physiological mechanisms including regulating metabolism, immune system,
354 stress, reproduction, growth, and development by acting on endocrine glands like the adrenal, gonads, and
355 thyroid (Lechan & Toni 2016, Rosol et al 2001, Kanda 2019, Zoeller et al 2007). Neurons from the
356 hypothalamus regulate the pituitary and downstream organs including the gonads, adrenal gland, and
357 thalamus by stimulating the release of neuropeptides conserved across bilaterians (Jékely 2013, Mirabeau
358 & Joly 2013, Bauknecht & Jékely 2015, Elphick & Mirabeau 2014, 2018). The *S. kowalevskii* genome
359 contains many of these conserved neuropeptides including vasotocin, orexin, gonadotropin-releasing
360 hormone (GnRH), corticotropin-releasing hormone (CRH), thyrotropin-releasing hormone (TRH), and
361 calcitonin (CalC), which have all been identified in previous studies (Mirabeau & Joly 2013, Jékely 2013,
362 Tian et al 2016, Semmens et al 2016). Vasotocin and orexin are two bilaterian-conserved neuropeptides
363 secreted in the hypothalamus in vertebrates. Vasotocin is expressed in scattered cells at the trunk in early
364 and late juveniles (Fig 3F,F'), whereas orexin is broadly expressed throughout the epithelium in early and
365 late juveniles, with minimal expression around the collar (Fig 3M,M'). GnRH stimulates secretion of
366 gonadotropins from pituitary neurons to regulate gametogenesis and gonadal development in both
367 vertebrates (Kawada et al 2013, Sakai et al 2017). In *S. kowalevskii*, GnRH neurons are located in
368 scattered cells at the proboscis base and in a similar domain to vasotocin at the trunk in early juveniles
369 (Fig 3I). Neurons in the trunk have a visible proximal projection into the plexus, shown in the in the inset
370 image (Fig 3I). Late juveniles have a strong ventral cord expression, with few cells along the dorsal cord
371 and dorsal proboscis base (Fig 3I'). Inset image shows the dorsal view with expression at the dorsal
372 proboscis base and along the dorsal cord in a late juvenile (Fig 3I'). CRH neurons in the vertebrate
373 hypothalamus signal to the anterior pituitary and stimulating the release of adrenocorticotropic hormone
374 into the bloodstream to regulate the stress response (Brunson et al 2013, Lovejoy et al 2014). CRH is
375 expressed throughout the proboscis in early juveniles (Fig 3L) and becomes restricted to the heart-kidney
376 complex overlying the stomocord and dorsal vessel, and along the dorsal cord in late juveniles (Fig 3L').

377 CalC and TRH are two additional HPA neuropeptides associated with thyroid function. CalC helps
378 control plasma calcium levels to regulate bone remodeling and metabolism in vertebrates (Zoeller et al
379 2007, Carter & Schipani 2006, Naot & Cornish 2008) and is thought to have an ancestral role in
380 regulating biomineralization (Cardoso et al 2020). CalC expression is seen in the posterior part of the
381 proboscis in scattered cells in both early and late juveniles (Fig 3N,N') and along the ventral cord in late
382 juveniles (Fig 3N'). Inset panel in Figure 3N show posterior projections of these neurons. TRH is
383 expressed in scattered cells in the anterior proboscis, strong expression in the dorsal proboscis base, and
384 along the trunk in early juveniles (Fig 3O). Cells at the trunk become restricted to the ventral cord in late
385 juveniles (Fig 3O'). In both early and late juveniles, there are two dominant cell clusters adjacent to the
386 dorsal proboscis base.
387
388 Other conserved neuropeptides within bilaterians include achatin and cholecystokinin (Elphick and
389 Mirabeau, 2014; Elphick et al., 2018; Jekely, 2013). Achatin shows restricted expression in large isolated
390 cells distributed in the anterior proboscis (Fig 3P,P'). Cholecystokinin (CCK) is a gastrointestinal
391 hormone peptide that has an ancient role in regulating feeding (Tinoco et al., 2021). CCK is expressed in
392 the proboscis base in early juveniles (Fig 3Q) and later has broader expression in the pharynx endoderm
393 and ventral trunk ectoderm in late juveniles (Fig 3Q').
394
395 Many of the neuropeptides show dense expression at the base of the proboscis so we tested whether there
396 was coexpression of multiple peptides, or each neural subtype associated with specific neuro peptides. We
397 performed multiplexed HCR for three peptides, NNFamide, TRH, and WFMRFamide (Fig 3R-R'''), all
398 expressed in similar domains. The anterior proboscis shows non-overlapping expression of the three
399 markers evenly distributed across the epithelium across both stages (Fig 3R,R''), and the posterior
400 proboscis is composed of non-overlapping rings of expression of individual neuropeptides (Fig 3R',R''').
401 The minimal neuropeptide coexpression suggests that neuropeptides may be good markers for specific
402 neural cell types in the proboscis.

403

404 Unlike neurotransmitters, which preferentially exhibit anterior expression, neuropeptides show more
405 extensive posterior expression along the ventral and dorsal cords. Expression data for neurotransmitter
406 and neuropeptide synthesis and transport markers suggests that *S. kowalevskii* has a strongly regionalized
407 nervous system, with an increased neural cell type diversity in 5 main territories; the anterior proboscis,
408 posterior proboscis, anterior collar, dorsal cord, ventral cord; but most prominently, the dorsal proboscis
409 base.

410

411 **Plexus and neural cord organization**

412 In the previous section we described the expression of many important genes involved in neural function
413 by *in situ* hybridization. These data provide useful information about specialization and location of
414 neuronal cell bodies, but tells us little about neural morphology, neurite and axonal projections, and the
415 general structure of the nervous system. To begin to investigate nervous system structure and function, we
416 performed immunohistochemistry for a monoclonal antibody (1E11) to the pan-neural marker
417 synaptotagmin, which was developed from the radial nerve extract of asteroid, *Asterina pectinifera*
418 (Nakajima et al., 2004b), to visualize cell morphology and neurite projections in juveniles and adults (Fig
419 4A). Previous comparative work has validated the cross reactivity of this antibody localizing to neurons in
420 other ambulacrarian taxa; broadly in echinoderms and in another species of hemichordate (Byrne et al.,
421 2007; Nakajima et al., 2004a).

422

423 Whole mount immunohistochemistry of late juveniles at the 3GS stage revealed a complex and structured
424 nervous system with a dense basiepithelial nerve plexus throughout the proboscis, but thicker at the base
425 (Fig 4A). Neurites and axons are well-labelled, but cell bodies had weak signal (Fig 4B). The plexus is
426 also very prominent in the collar ectoderm, but much less in the trunk. An endodermal plexus is visible
427 throughout the pharynx. The subepidermal collar cord is clearly visible extending from the thick plexus at

428 the dorsal posterior ectoderm of the proboscis into the superficial dorsal cord, which begins in the
429 posterior collar and runs the length of the trunk terminating at the anus. The wider superficial ventral cord
430 begins at the posterior collar/anterior trunk boundary and extends posteriorly throughout the entire ventral
431 midline of the animal.
432
433 We further utilized 1E11 to determine the structure of the nervous system in adults. As many of the neural
434 cell type markers exhibit localized domains of expression in the proboscis, we first investigated 1E11
435 expression at this site. We examined the plexus in this territory by peeling off sections of ectoderm from
436 the underlying proboscis mesoderm in fixed adults and carrying out whole mount immunohistochemistry
437 on these tissue fragments (Fig 4C). In the general proboscis ectoderm, we observe a well-organized
438 plexus with parallel bundles of processes running along the AP axis, with regularly spaced connectors
439 projecting laterally between the bundles (Fig 4D). This organization is remarkably similar to the drawings
440 of Knight-Jones (1952). The dorsal superficial cord is visible as a thickening of this plexus (Fig 4E). The
441 neurite bundles projecting along the AP axis observed in the mid proboscis exhibit a striking transition in
442 plexus structure: a complex architecture of thicker neurite bundles forming a series of layered,
443 interconnected tracks. This can be clearly observed in Figure 4D where the flat mount of the ectoderm
444 shows the parallel projections on the left of the panel projecting into the complex plexus at the proboscis
445 base at the right of the panel. A z-stack of this territory more clearly shows the structure of the plexus
446 (Supplementary Movie 1). Higher magnification shows the complex architecture of this territory (Fig
447 4F,G). The structure of this domain is very reminiscent of the anterior territory of the plexus structure in
448 the acoel *Hofstenia miamia* (Hulett et al., 2020) and the holes in the plexus may represent extensions from
449 epithelial cells that attach to the basement membrane as reported from early EM studies (Dilly, 1969).
450 Moving posteriorly into the collar, we observed a similar, structured plexus to the proboscis base, but
451 with less densely packed tracts (Fig 4H). A z-stack (Supplemental Movie 2) in this region again clearly
452 shows the structured nature of this plexus. Further posterior in the trunk, the plexus is less extensive than

453 in the proboscis or collar, with the dorsal and ventral cords being the most prominent features
454 representing condensations of the plexus along both midlines (Fig 4I).
455
456 The results from 1E11 reveal many general aspects of the distribution and organization of the neural
457 plexus, but little resolution of individual neurites. We used injection of lipophilic dye (DiI) into adult
458 fixed tissue in the mid proboscis to look more closely at the morphology and directionality of neurite
459 projections. Individual neurites extend from the injection site in all directions, but with prominent neurite
460 bundles projecting along an AP axis, matching what was observed with the IE11 antibody (Fig 4J,K). The
461 plexus is clearly structured, with the imaging stacks showing different projection patterns according to the
462 position along the apico/basal axis in the plexus. Lower volume injections of DiI imaged at higher
463 magnification reveal many neurites with regular puncta along their length (Fig 4L,M). As these swellings
464 may represent fixation artifacts, we utilized a live neural stain, NeuO, a membrane-permeable fluorescent
465 probe (Er et al., 2015). We observe similarly labeled neurites/axons in the trunk revealing regularly
466 spaced boutons along the neurites/axons (Fig 4N). The similar structures detected along the processes
467 using both fixed (DiI) and live (NeuO) tissue suggest these structures may represent either *en passant*
468 synapses (de Castro, 1950), or varicosities involved in volumetric release (Nieuwenhuys, 2000).
469

470 **Morphology and projection of neural subtypes**

471 Our *in situ* hybridization data for neurotransmitter and neuropeptide synthesis and transport markers
472 clearly demonstrates that *S. kowalevskii* has strong regional specialization of its nervous system, and also
473 revealed the location of cell bodies characterized by specific neurotransmitters and neuropeptides.
474 However, these data provide no information about the directionality or length of projections, and *in situ*
475 hybridization data rarely provides information about cellular morphology. We used two different methods
476 to investigate details of neural subtype morphology and projections; cross reactive antisera to
477 neurotransmitters and neural transgenics.

478

479 **Cross reactive antisera**

480 **Serotonergic neurons**: We used an antibody raised to 5-HT to label serotonergic neurons in 3GS stage *S.*
481 *kowalevskii* (Fig 5A). Previous work using this antibody has already investigated the distribution of the
482 serotonergic nervous system in early developmental stages, in juveniles and limited sections in adults, and
483 our data confirms expression and extends sampling of these studies (Brown et al., 2008; Cunningham and
484 Casey, 2014; Kaul-Strehlow et al., 2015). Figure 5 shows the distribution of the serotonergic nervous
485 system in juveniles and adults. In juveniles, the serotonergic nervous system is composed of primarily
486 receptor, flask-shaped bipolar neurons broadly dispersed in the proboscis ectoderm and collar, but more
487 sparsely in the trunk. In the proboscis, while staining is broadly scattered, there are no cell bodies detected
488 in either the most apical ectoderm or at the base of the proboscis (Fig 5A,C). All neurons project into the
489 underlying neural plexus, although it is not possible to trace the full length of individual axons due to
490 large numbers of projections in the plexus. However, proboscis neurons appear to generally project
491 posteriorly, based on the orientation of the axon close to the cell body. In the collar, cell bodies are
492 organized into three rings, two at the anterior and one at the mid collar (Fig 5A,D). These neurons also
493 have a single dendrite and sensory cilium projecting out of the epithelium, and a single axon projecting
494 basally into the neural plexus. There are positional differences in cell body location within the epithelium;
495 some cell bodies are located basally and others more apically (Fig 5B). In the collar and proboscis, we see
496 no dorsoventral differences in the distribution of cell bodies, however, cell bodies in the trunk are
497 positioned on the dorsal side, mostly lateral to the dorsal cord but generally project ventrally into the
498 ventral cord (Fig 5E). In the anterior part of the trunk, there are also cell bodies scattered in the ectoderm
499 more laterally around the gill slits (Fig 5A). A z-stack of the serotonergic nervous system in this region
500 again clearly shows the structured nature of this plexus, as well as dorsal sensory cells projecting laterally
501 along the trunk towards the ventral cord (Supplementary Movie 2).

502

503 We further extended our analysis into adult animals. Whole mount immunohistochemistry in adults show
504 a far more extensive serotonergic population than in juveniles but generally confirm a similar expression
505 pattern established in juveniles. Figure 5F shows a view of the mid-proboscis, showing broad distribution
506 cell bodies projecting into the underlying epithelium, with projections in all directions, but most
507 projecting posteriorly, similar to the organization revealed from 1E11 (Fig 4E). The base of the proboscis
508 (the same specimen as Fig 4D,E) double labelled for both 1E11 and 5HT (Fig 5G,H) reveals that
509 serotonergic axons form a subset of the complex network of bundles. The morphology of the neurites
510 shows swellings along the length of the processes similar to what we demonstrated with DiI labelling. In
511 the collar (Fig 5I), staining is absent in the anterior lip, but just posterior there is a ring of expression in
512 the ectoderm, and broad ectodermal labelling throughout the collar ectoderm. Cell bodies are more
513 broadly dispersed throughout the collar epithelium, rather than in discrete rings as in 3GS juveniles. Note
514 that these findings contrast with the lack of neural staining from *elav* in this region (Fig 1). In the
515 posterior trunk, the epithelium is ruffled, and we observed patches of cell bodies in the lateral body wall,
516 and an extensive, but thin, plexus throughout the trunk epithelium (Fig 5J).
517
518 We next investigated the labelling of the serotonergic neurons in representative cross sections along the
519 adult body, counterstained with phalloidin (Fig 5K). In the posterior proboscis, we observe clear
520 dorsoventral asymmetry in plexus thickness, with the dorsal region thicker than the ventral territory, and
521 with cell bodies distributed more ventrally in this plane of section (Fig 5L). In the mid-collar (Fig 5M) the
522 neural plexus is extensive in both the ectoderm and the endoderm but is thinner than the proboscis plexus
523 (Fig 5L). The dorsal cord is clearly visible and shown in higher magnification in Fig 5N: DAPI labels the
524 soma of the cord positioned above the neurites that project through the cord, and as reported elsewhere,
525 there is no obvious cord lumen. We did not observe any 5HT+ cell bodies in the cord soma in the limited
526 sections we examined. As observed in the whole mount (Fig 5M), there is a broad distribution of cell
527 bodies projecting into the plexus, without any dorsoventral differences. The pharyngeal epithelium also
528 shows a prominent plexus throughout the pharynx, yet only a few isolated cell bodies are associated with

529 the endoderm in these sections. Sections in the anterior trunk show cell bodies sparsely scattered
530 throughout the ectoderm with a thin ectodermal plexus that thickens ventrally, and the dorsal cord
531 showing far fewer axons labelled than in the ventral cord. The endodermal plexus is very sparse (Fig 5O).
532 In the posterior trunk, labelling of axons in the ventral cord is more prominent and a thin plexus is
533 detected throughout the epithelium with scattered, isolated cell bodies (Fig 5P,Q). No endodermal plexus
534 was detected.
535
536 **GABAergic neurons**: We used a GABA polyclonal antibody to stain GABAergic neurons in juveniles,
537 as has been previously demonstrated in another enteropneust species, *P. flava* (Nomaksteinsky et al.,
538 2009). To address concerns about antibody binding specificity, we compared GABA antisera reactivity
539 with the *in situ* hybridization for GAD (Fig 2). We observed good concordance between the antibody and
540 *in situ* hybridization localizations. The GABAergic nervous system in juveniles is concentrated both in
541 the anterior and posterior proboscis ectoderm (Fig 6A,Ai). In the collar, there are two ectodermal rings of
542 cells at the lip of the collar (Fig 6A). In the trunk, there are isolated neurons along the dorsal midline in
543 both the ectoderm and endoderm (Fig 6Aii). These cells appear similar in morphology to 5HT+ cells;
544 bipolar with a single neurite extending from the cell body to the apical region terminating with an apical
545 cilium, and the axon descending into the plexus on the basal side. There are also dorsal endodermal
546 neurons with a neurite projecting to the apical surface of the endoderm, but with the cell body embedded
547 in the endodermal plexus (Fig 6Aii). Further posteriorly, there are prominent axonal projections around
548 the gill slits and into the ventral cord (Fig 56iii).
549
550 The number of cell bodies at the proboscis, collar, and trunk increases substantially in adults. The base of
551 the proboscis forms a similar pattern of GABA+ neurite bundles to those detected from 1E11 and 5HT
552 (Fig 6B). The adult collar has a more expansive concentration of neurons with the anterior ring and
553 scattered cell bodies throughout the collar ectoderm (Fig 6C). GABAergic neurons are labeled in gill bars
554 (Fig 6D) with cell bodies projecting axons ventrally. To directly image the dorsal cord, we dissected the

555 cord from the ectodermal tissue, keeping the nerve bundles intact. This revealed many neurites projecting
556 in an anterior-to-posterior direction along the length of the cord, with some neurites projecting laterally
557 (Fig 6E).
558
559 **FMRFamidergic neurons:** We used the rabbit polyclonal anti-FMRFamide to identify potential
560 FMRFamidergic neurons in 3GS stage embryos. This antibody has been shown to be cross-reactive in a
561 diverse set of bilaterians including echinoderms, where reactivity is observed in the radial nerve cord,
562 tube feet, apical muscle, intestine, and the esophagus nerve plexus (Hoekstra et al., 2012). While the exact
563 epitope that is recognized is uncertain, some studies have also found that the FMRFamide antibody
564 exhibits cross-reactivity with SALMFamides and GFSKLYFamide in the sea cucumbers (Ajayi and
565 Withyachumnarnkul, 2013; Diaz-Miranda et al., 1995). Therefore, the possible affinity to other
566 neuropeptides must be considered in *S. kowalevskii.* The labelling shows significant overlap with the *in*
567 *situ* data for PC2 and GPC, the two enzymes involved in the processing of neuropeptides, so this data
568 provides information about the projection of a subset of neuropeptides within the complement in *S.*
569 *kowalevskii*.
570
571 The peptidergic labelling from this antibody shows a broad circumferential distribution of neurons in the
572 proboscis, but with a concentration at the proboscis base of both cell bodies and axons (Fig 6F). Neurons
573 at the proboscis base have a flask-shaped morphology like the morphology of many other neurons
574 described in this study, with a single cilium extending into the outer ectoderm (Fig 6F). These neurons
575 appear to project posteriorly down the proboscis stem and along the dorsal collar cord, with some
576 projections following the nerve plexus along the collar epithelium (Fig 6F, Fi) connecting with the ventral
577 cord along the trunk (Fig 6F). Cell bodies are detected in the ventral cord with axons running the length of
578 the cord. In the postanal tail of the juvenile, axons are clearly projecting anteriorly (Fig 6Fii). We
579 examined labelling of the adult nervous system by dissection of the ectoderm from the mesoderm in the
580 proboscis and imaged the plexus (Fig 6G). This revealed an extensive plexus throughout the proboscis

581 ectoderm with a general trend of bundled projections along the AP axis, but with many lateral neurites
582 connecting these bundles projecting both long and short distances.
583

584 **Neural transgenes**

585 **Synapsin transgene:** To visualize neurons in higher resolution, we generated a Synapsin construct to
586 drive expression of eGFP. Synapsin is a synaptic vesicle transmembrane protein and a marker of
587 differentiated neurons (De Camilli et al., 1983; Huttner et al., 1983). Our construct was designed using 8
588 kilobases (KB) upstream of the start site of the synapsin-2-like gene (XP_006820290.1) (Minor et al.,
589 2019). We examined transgene expression in over 50 F_0 juveniles at a range of developmental stages. The
590 transgenic animals exhibit mosaic incorporation of the transgene and show neuronal staining most
591 prominently throughout the proboscis ectoderm, sometimes in the dorsal region of the trunk and collar in
592 isolated neurons (Fig 7A, B). Because of the mosaicism, transgenic animals ranged from a single labeled
593 neuron to hundreds of labeled cells. From these transgenics animals, we identified the range of neural
594 morphologies and the length and directionality of their neural processes. The most common neural
595 morphology we observed with this transgene were large bipolar sensory neurons, like those observed with
596 5HT immunohistochemistry. We found these neurons throughout the ectoderm, but at highest density in
597 the proboscis. In a separate synapsin:GFP juveniles, we detect large bipolar neurons in the anterior tip of
598 the proboscis projecting posteriorly towards the proboscis base (Fig 7B). At the dorsal proboscis base,
599 neurons have a flask-shape morphology, with a rounded nucleus close to the neural plexus, and with
600 either a single axon, white arrow in inset, or an axon that splits into an anteriorly and posteriorly
601 projecting extension, grey arrow in inset (Fig 7Aii). We also identified a group of elongated sensory
602 neurons in the posterior collar with a single axon projecting anteriorly into the cord, white arrows (Fig
603 7Aiii). Similar neural morphology was detected in the posterior ectoderm with clear anterior projections
604 (Fig 7Aiv). The projections of this group of neurons are likely involved in relaying posterior sensory

605 information from the trunk to the anterior part of the animal with most axonal termini at the base of the
606 proboscis. We rarely detected unipolar neurons, but one is shown associated with the plexus projecting
607 anteriorly into the dorsal cord towards the proboscis, grey arrow (Fig 7Aiii). Elongated bipolar neurons
608 are detected in the far posterior ectoderm and project anteriorly along the dorsal midline, likely along the
609 dorsal cord (Fig 7Aiv).
610
611 Many of the bipolar neurons have prominent swellings along the axons projecting into the basiepithelial
612 plexus (Fig 7Bi) like what we reported for DiI and serotonin. Many of these varicosities are located close
613 to the basement membrane of the plexus, so it is possible that they may be acting in a paracrine fashion,
614 releasing transmitters/peptides locally, modulating other neurons, directly stimulating muscles through
615 the basement membrane, or representing *en passant* synapses within the plexus. In some cases, we detect
616 what we interpret to be interneurons, closely associated with the neural plexus, co-labelled with DAPI
617 (Fig 7Bii). We also find neurons with a more circular cell body morphology along the mid-proboscis that
618 project anteriorly (Fig 7Biii). In this juvenile, bipolar neurons in the proboscis project posteriorly and
619 appear to terminate at the proboscis base rather than extending further posteriorly (Fig 7B). In other
620 transgenic juveniles, the population of bipolar neurons, right above the first gill slit in the anterior dorsal
621 midline trunk, project anteriorly and terminate at the dorsal proboscis base in many of the animals that
622 were imaged (Fig 7C).
623
624 Overall, based on the data from this synapsin transgene, the *S. kowalevskii* ectoderm contains a range of
625 neural cell types including pseudounipolar, bipolar, multipolar, and multiciliated neurons in the proboscis
626 and collar (Fig 7D-G). However, by far the most prevalent type of labeled neuron is the bipolar
627 morphology observed throughout the animal. The abundant bipolar neurons are distinguishable from
628 other types of cells in the ectoderm because of the distinctive axonal projections into the plexus.
629

630 **Location of transmitter release**: eGFP+ neurons from the transgene, DiI staining on fixed tissue, and
631 NeuO labeling in live tissue, all reveal the presence of varicosities along the axons for most of the
632 labelled neurons, most likely the site of transmitter/peptide release, possibly resulting in volumetric
633 transmission or as *en passant* synapses. To further test this and to determine the localization of
634 synapses/transmitter release throughout the nervous system, we designed a construct based on the
635 previous synapsin:eGFP from Figure 7, but with the addition of a mouse synaptophysin-mRuby fusion
636 protein. Synaptophysin is a presynaptic vesicle protein (Pennuto et al., 2003; Wiedenmann and Franke,
637 1985), so we expect the fusion protein to be transported to either synapses or regions of vesicle release, as
638 has been demonstrated in mouse using a similar construct (Beier et al., 2015). The transgene generates
639 mosaic eGFP expression similar to data presented in Figure 7 (Fig 8A,E). Within these eGFP-labelled
640 neurons, we detect puncta labelled with mRuby, suggesting that the mouse Synaptophysin is trafficked
641 successfully in hemichordates and labels regions of transmitter/peptide release. In the anterior proboscis
642 (Fig 8B), there are many synaptophysin puncta along axons in addition to axon terminus containing a
643 concentration of the synaptophysin fusion protein (Fig 8B,C,D). We observe broad distribution of these
644 puncta in both the anterior (Fig 8B) and posterior proboscis (Fig 8C). Synaptophysin also shows
645 localization around the nucleus and along the cilium in bipolar neurons (Fig 8D). In one striking example,
646 we were able to track a single axon from a cell body in the far posterior to the mid proboscis (Fig 8E).
647 Regular localization of Synaptophysin in swellings along the length of the axon supports our previous
648 suggestion that the neuron is secreting transmitters/peptides locally or making direct neuron-to-neuron
649 connections in the trunk plexus (Fig 8F-H).
650
651 **Tyrosine hydroxylase transgene:** To investigate the cellular morphology and projections of
652 catecholaminargic neurons, we designed a transgene using 5KB of sequence directly upstream of the
653 tyrosine hydroxylase gene. Previously, we established that the cells expressing TH in the proboscis and
654 collar also expressed the dopamine transporter (DAT) supporting the hypothesis that catecholaminergic
655 TH-expressing cells are dopaminergic neurons (Fig 2). The TH:eGFP transgene expression is again

656 expressed mosaically and mainly restricted to the proboscis, with a few isolated cells in the posterior
657 collar (Fig 9A). Many of the labelled neurons in the proboscis have a flask-shaped morphology, as
658 reported for synapsin:eGFP, and contain a single axonal projection directly into the plexus (Fig
659 9B,C,F,F'). In about half of the animals imaged, we identified a unique type of cell at the posterior collar
660 and in many cases were able to trace their projections (Fig 9D,E). They have a unique asymmetric cellular
661 morphology; a single dendrite with a terminal sensory cilium, and a protruding vacuole-rich mass. These
662 cells have elaborate axonal trajectories across the collar and often project anteriorly into the proboscis
663 (Fig 9G-I'). Individual neurons were traced and 3D-reconstructed using the 3D Visualization-Assisted
664 Analysis (Vaa3D) software suite. TH transgene-labelled neurons in the anterior proboscis project
665 posteriorly towards the proboscis base (Fig 9F,F') whereas eGFP+ neurons at the proboscis base project
666 anteriorly towards the proboscis tip (Fig 9J-K'). Outside of the proboscis in the few eGFP+ neurons in the
667 collar, neurons project anteriorly towards the proboscis base (Fig 9G-I').
668
669 In summary, the transgenic data reveal the detailed cellular morphology of neurons across different
670 regions of the body plan, and for the most part, neurons have a similar morphology; bipolar sensory
671 neurons that project into the neural plexus and often at long distances. Far fewer neurons with detected
672 with more diverse morphologies that were described in classical studies.
673

674 ## Discussion

675

676 **Distribution of neurons and neural cell types in *S. kowalevskii***

677 The expression of a wide range of molecular markers of neurons and neural subtypes in *S. kowalevskii*
678 confirms the broad distribution of neurons in the ectoderm outlined in several classical descriptions
679 (Knight-Jones 1952, Bullock, 1940; Bullock, 1945; Hess, 1937). However, unlike the simple neural

680 plexus proposed by Bullock (1945), our data suggests that the nervous system of enteropneusts is far from
681 simple. The few molecular studies in hemichordate neural structure and organization have focused on the
682 distribution of neurons in the cords, in particular the dorsal cord due to its proposed affinities with the
683 chordate dorsal cord (Nomaksteinsky et al., 2009, Miyamoto and Wada, 2013). Our study provides
684 additional insights, by investigating the entire nervous system including both the cords and the extensive
685 neural plexus. The data clearly identifies a complex arrangement of spatially segregated neural subtypes
686 that is most prominent in the general ectoderm rather than in either cord. The proboscis epithelium is the
687 most richly innervated region of the animal, particularly at the base and close to the proboscis stem on the
688 dorsal side, as has been described in other species of enteropneust (Nomaksteinsky et al., 2009). The
689 collar ectoderm is quite densely populated with neurons but the trunk far less so, but neurons are also
690 concentrated along the midlines in both the dorsal and ventral cords (Fig 1P,S). Data from *elav*, widely
691 used as a pan neural marker, does not seem to label all the neural complement, as some neurons in the
692 epithelium are not *elav*+ as shown by the extensive expression of 5HT in the collar epithelium (Fig 5I).
693
694 The strongly regionalized distribution of neural subtype markers in the epithelium of both classical
695 neurotransmitters and peptidergic neurons suggests that there is marked differentiation of the nervous
696 system in both the AP and DV axes (Fig 2,3). At the late juvenile stages, we observed strong
697 regionalization of specific neural markers, densely packed and largely expressed in distinct rings,
698 predominantly in the anterior plexus. However, we also saw evidence of clear molecular differentiation of
699 neural subtypes between the dorsal and ventral cords, but in relatively few markers when compared with
700 expression in the plexus. These data provide a broader view of neural cell type specification throughout
701 the body plan rather than uniquely on cord differentiation (Miyamoto et al., 2010; Miyamoto and Wada,
702 2013; Nomaksteinsky et al., 2009).
703
704 **Cell type regionalization in the general ectoderm**: We observed the most complex regionalized patterns
705 in the proboscis and collar epithelium, and far fewer in the trunk. However, far from the simple nervous

706 system proposed by Bullock (1945), our molecular analysis suggests a highly regionalized nervous
707 system with a particularly complex organization at the base of the proboscis: there were three general
708 expression domains; apically restricted, broadly expressed, and localized to the base, with some markers
709 represented in multiple domains. Most of these neural populations show circumferential domains with
710 little evidence of dorsoventral differentiation reflective of the structure of the plexus. The base of the
711 proboscis is both the region of highest neural density and the most diverse in terms of neural cell types.
712 Dopaminergic (DA), GABAergic, histaminergic, and peptidergic neurons show circumferentially
713 localized domains of expression in this region (Fig 2,3), and as we also demonstrate, it is also one of the
714 most distinctive regions of neural plexus organization (Fig 4). The expression of GABA in the proboscis
715 of *P. flava* exhibited a similar distribution to our findings, although their focus was largely restricted to
716 the base of the proboscis and stem (Nomaksteinsky et al., 2009). In the collar, the diversity and density of
717 neurons is less than in the proboscis, and in the trunk of late juveniles, the only 2 neural subtypes
718 represented in the general ectoderm of late juveniles, not associated with the cords, are serotonin and DA.
719
720 The rings of neural subtypes in both the collar and proboscis ectoderm are very similar to the expression
721 domains of the regulatory genes with conserved bilaterian roles in CNS patterning described in previous
722 studies on *S. kowalevski* and other enteropneusts species (Kaul-Strehlow et al., 2017; Lowe et al., 2003;
723 Pani et al., 2012). What is particularly striking is the clustering of neural subtypes in the regions of the
724 ectoderm that are the sites of localized epithelial signaling centers during early development. The apical
725 tip of the developing proboscis is the site of active FGF and Hedgehog (Hh) signaling, and a source of
726 Wnt antagonists (Darras et al., 2018; Pani et al., 2012). This territory and has been compared to the
727 vertebrate anterior neural ridge. We observe a wide range of neural subtypes clustered in this region. At
728 early developmental stages, the boundary between the proboscis and collar is the site of a narrow
729 circumferential stripe of transitory Hh expression that strongly resembles the regulatory gene expression
730 profiles of the vertebrate Zona Limitans intrathalamica (ZLI). We notably observed a tight localization of
731 GABA and DA neurons clustered in this region on either side of this organizer. Finally, the boundary of

732 the collar and trunk is the site of the expression of Wnt1 and FGF8, which are the characteristic ligands of
733 the isthmus organizer at the midbrain hindbrain organizer. This is a key organizer for the formation of the
734 midbrain dopaminergic neurons in vertebrates, and both TH *in situs* and transgenics show TH neurons in
735 this general region. Further functional tests will be required to determine whether these conserved
736 regulatory networks are involved in the regulation of specific neural subtypes in these territories but raises
737 the exciting possibility that conservation of gene regulatory networks between these disparate body plans
738 is related to their role in the positioning of conserved cell types along the AP axis.
739
740 **Origins of hypothalamus and pituitary**: The clustering of neurons around the base of the proboscis that
741 express orthologues of neuropeptides/neurohormones that are involved in the function of the
742 hypothalamic/pituitary axis in vertebrates is of particular interest. Evolutionary insights into the origins of
743 the neurosecretory centers of the vertebrate brain have come from Amphioxus and tunicates, but little is
744 known outside of chordates (Zhang and Ji 2022, Lemaire et al 2021). Studies from the annelid *Platynereis*
745 *dumerilii* have demonstrated a potential hypothalamic precursor suggesting a deep ancestry of
746 neurosecretory centers in bilaterians (Tessmar-Raible et al., 2007, Denes et al., 2007). Echinoderms and
747 hemichordates have largely been excluded from a broader synthesis, except for the early pioneering
748 studies by Bateson (1885) who compared the proboscis pore at the dorsal base of the proboscis to
749 Hatschek's pit in amphioxus linking it to pituitary and hypothalamic origins, and Komai (1951) who
750 compared the stomocord to the pituitary. The expression of many of the orthologues of characteristic
751 neuropeptides/neurohormones of the hypothalamus (TH, GnRH, CRH, CalC, Orexin) around the base of
752 the proboscis suggest that a more rigorous investigation of this region is warranted to investigate the
753 projections of the neurons expressing neurohormones to determine whether they project to a similar
754 region and whether this territory represents a basic neurosecretory center. Strikingly, the regulatory gene
755 *pitx* (pituitary homeobox) is expressed in a prominent spot at the base of the proboscis (Lowe et al 2006),

756 and given the regulatory program of both the hypothalamus (Xie and Dorsky 2017) and pituitary is well
757 characterized, this should be investigated in parallel.
758
759 **Cell type regionalization in the cords**: Both the dorsal and ventral cords show characteristic expression
760 domains of specific neural cell types. However, we detect the expression of only a subset of the markers
761 that we see prominently expressed in the proboscis. Despite fewer neural subtypes, those that are
762 expressed show that the cords are distinct molecularly, suggesting differentiation of function. Given our
763 analysis was largely restricted to late juveniles, it is possible that the complement of neural subtypes
764 expands as the animals grow larger. The dorsal cord is divided into the internalized collar cord, and
765 superficial cord than runs the length of the trunk to the anus. We see little evidence of any
766 neurotransmitter marker expression in the collar cord soma, except for peptidergic neurons, despite the
767 prominent expression of *elav*. In the more posterior domains, where the cord is superficial and
768 basiepidermal along the trunk, there are glutamatergic neurons that run down either side of the dorsal
769 cord, and a few isolated GABA labelled cells in the anterior portion of the dorsal cord. Both cords, show
770 clear expression of peptidergic neurons based on the expression of the processing enzymes and several
771 neuropeptides. The length of the ventral cord shows strong and broad expression of the histidine marker
772 HDC.
773
774 When the expression of a wide range of markers of neural differentiation are considered, in both the
775 epidermis and in the cords, we see that most neurons at the late juvenile stage are in the proboscis
776 ectoderm rather than in the cords. The region of the highest neural density and diversity is in the
777 proboscis ectoderm, around the base. A previous study in *P. flava* (Nomaksteinsky et al., 2009) had
778 identified the proboscis stem as a region with strong neural differentiation, and we confirm this, but we
779 would include the entire proboscis base in this region of rich neural diversity rather than just the dorsal
780 territory. Many of the gene expression domains in this region are organized in circular rings reminiscent

781 of the expression of nested transcription factors with key roles in neural cell fate determination in
782 vertebrate brain development.
783
784 **General organizational features of the plexus and cords:** Previous studies have revealed the pervasive
785 plexus present throughout the epidermis, and our data further refines the structural details of the plexus
786 adding significant details (Bullock, 1945; Knight-Jones, 1952; Silèn, 1950; Spengel, 1877, 1903). The
787 plexus is more prominent in the proboscis and with a striking change in organization at the proboscis
788 base, where its organization transitions from parallel nerve bundles running along the AP axis, into a
789 mesh of axonal bundles containing both serotonergic, GABAergic, and peptidergic processes (Fig. 4). A
790 very similar plexus structure has recently been reported in different acoel species (Hulett et al., 2020). In
791 these cases, it is reported that the reticulated neurite bundles wrap around cell clusters. Dilly (1969)
792 reported that the enteropneust epithelium is strongly bound to the basement membrane by cellular
793 processes that penetrate this plexus, so it is possible that this territory has its distinctive morphology due
794 to cells penetrating and attaching to the basement membrane. The plexus is much thicker at the proboscis
795 base and is most prominent on the dorsal side and possibly represents a center of integration
796 (Nomaksteinsky et al., 2009). While this structure is most striking at the base of the proboscis, a looser
797 mesh of axonal bundles is also present in the collar. Confocal z-stacks of the plexus, stained with neural
798 antibodies or following DiI labelling, show that the plexus clearly has some apico/basal structural
799 organization throughout the proboscis and collar suggestive of a partitioning of function – a scenario
800 explicitly rejected in classical studies (Bullock, 1945).
801
802 Data from the transgenic embryos give particularly valuable insights into the structure of the plexus, as
803 the mosaic incorporation of the transgene labels only a subset of neurons and enables the tracking of
804 individual neurites. We see no evidence of a plexus organization like that of the simple nets of cnidarians,
805 in which local projections synapse directly to neighboring neurons. Instead, we largely observe long range
806 projections from sensory neurons in the epithelium. Neurons in the anterior proboscis mostly project

807 posteriorly to the base of the proboscis. However, there is a wide range of axonal trajectories observed,
808 and at the base of the proboscis we observed mostly lateral projections, but also some projections
809 anteriorly. The few cells labelled in the trunk project anteriorly into the proboscis. In some experimental
810 embryos, we were able to trace the neurite from the tip of the tail all the way up to the base of the
811 proboscis, suggesting very long-range communication in the animal (Fig. 6E). We were unable to find a
812 single instance of the axonal projections crossing the basement membrane and into the muscles, from
813 either immunohistochemistry or transgenic data, representing a wide range of neural subtypes. This
814 finding is significant as there has been some disagreement in the classical papers as to whether there is
815 direct innervation of muscles and evidence of axonal processes crossing the basement membrane,
816 summarized most recently by Dilly (1969). Light microscopy reports were decidedly mixed in their
817 assessments with some confirming axonal crossings, but mostly were cautious and reserved in drawing
818 conclusions (Bullock, 1945; Horst, 1939; Knight-Jones, 1952; Silèn, 1950). In Hyman's invertebrate
819 treatise, she concluded there was no compelling evidence for fibers crossing the basement membrane
820 (Hyman, 1955). With the advent of electron microscopy this issue was revisited: two independent studies
821 suggest direct innervation of muscles from fibers crossing the basement membrane (Dilly, 1969;
822 Nørrevang, 1965), but neither study report evidence of neuromuscular junctions. This question would
823 clearly benefit from further clarification using modern serial approaches such as serial block face SEM
824 (Lippens et al., 2019). Comprehensive examination of the sister group to hemichordate, the echinoderms,
825 has shown a similar lack of direct muscular innervation and penetration of the basement membrane by
826 neural fibers in any echinoderm group examined (Cobb and Pentreath, 1977, 1978; Nieuwenhuys, 2000).
827 Even in chordates, Amphioxus, the most basally branching chordate lineages, muscle fibers extend to the
828 neural tube and stimulation occurs at this basement membrane interface (Flood, 1966), suggesting that
829 sophisticated animal behavior can be mediated without a direct neuromuscular junction.

830 Our data further provides insights into the potential predominant mode of neural transmission in *S.*
831 *kowalevskii*. The transgene and DiI data are particularly informative: all axons observed at high

832 magnification were characterized by regular varicosities along their length. One striking synapsin
833 transgenic embryo showed regularly spaced varicosities along the axon of a single neuron from the tail all
834 the way up into the base of the proboscis (Fig 8E-H)). Synaptophysin protein localized to the varicosities
835 suggesting that transmitter/neuropeptide release occurs along the length of the neuron. Varicosities were
836 also pervasive in the proboscis neurons lending support to the idea that, like in echinoderms,
837 communication may largely be paracrine across the plexus, with general transmitter/neuropeptide
838 volumetric release. Volumetric transmission is recognized as a critical component of a wide range of
839 neural systems from the simple to the more complex (Descarries et al., 2008; Descarries et al., 1997;
840 Descarries and Mechawar, 2000; Nicholson, 2000; Nieuwenhuys, 2000). In many extant nervous systems,
841 from vertebrates to *C. elegans* and marine larvae, paracrine, chemically wired brain centers are integrated
842 with synaptic networks, and some authors have proposed that most extant nervous systems likely evolved
843 from peptidergic, paracrine systems (Jekely, 2021). We propose that during the early ambulacrarian
844 evolution paracrine signaling was evolutionarily favored as the predominant mode of neural transmission.
845 We cannot rule out the presence of true synapses between neurons in the plexus and the cords, but at least
846 in the juveniles we examined the presence of neuromuscular junctions is unlikely, and we saw no
847 evidence of the presence of axonal processes crossing the basement membrane into the muscle as was
848 reported by early EM studies (Dilly, 1969). However, it is possible that these develop as the animals grow
849 larger. Nieuwenhuys from his review of volumetric transmission across animal groups (Nieuwenhuys,
850 2000) makes the key statement that "the notion that volume transmission is primitive, generalized,
851 sluggish and lacks precision, whereas wiring transmission is advanced, specialized, fast and accurate, is
852 erroneous." Our data needs to be corroborated by neurophysiological assays to determine the function of
853 the nervous system in enteropneusts, but already sets up some clear hypotheses that can be further tested
854 by some targeted serial EM to investigate the detailed structure in the plexus at a variety of regions of the
855 body plan. Of course, this is a description of a single species representing one family of enteropneusts.
856 Follow up studies in additional species, representing a broader range of diversity, will be required to

857 determine whether the details of *S. kowalevskii* neuroanatomy adequately represents the main
858 organizational features of enteropneusts.

859 **Central or decentralized nervous system**

860 Much of the comparative interest in enteropneusts has been in its potential to provide insights into the
861 early origins of chordates. The structure of the nervous system is a critical character for inferring ancestral
862 states of early deuterostome nervous system (Holland et al., 2015). Our data provides some insights into
863 this question, but also raises many others. A simple statement to satisfy whether enteropneusts are
864 characterized by a central nervous system clearly delineated from a peripheral nervous system seems
865 largely driven by our expectations based on studies from highly derived, cephalized model animals. Our
866 data does not provide a clear answer to the question.
867
868 The transgenic animals are the most informative on this issue as they reveal that the predominant neural
869 cell type is a bipolar sensory neuron that project long distances, both in the proboscis and in the trunk. We
870 found scant evidence of the multipolar neurons described in classical studies at the basal side of the
871 plexus. In a few animals, we identified what we interpreted as a potential interneuron close to the
872 predominant bipolar sensory neurons in the tip of the proboscis, and a few instances of multipolar neurons
873 in the proboscis plexus (Fig 7). From our data so far, it is difficult to delineate a distinction between a
874 clearly defined central nervous system and a peripheral nervous system. A previous molecular study
875 (Nomaksteinsky et al., 2009) concluded that the dorsal cord and proboscis stem represented a "bonafide
876 CNS" and the rest of the proboscis and remaining epithelium was a peripheral nervous system. Our data
877 does not support such a strong division, as most neurons identified are sensory, with few candidates for
878 interneurons. At least at this juvenile stage, a division between peripheral and central is not obvious, and
879 the varicosities throughout the plexus are likely involved in processing sensory information. Our data
880 does support an important role of the dorsal proboscis stem as a region of potential integration
881 (Nomaksteinsky et al., 2009), as we observe many of axonal processes from transgenic embryos

projecting to this region consistent with previous hypotheses, but the entire proboscis base may be a region of integration rather than simply the dorsal side. We find little support for a special role of the dorsal cord as an integrative center, but perhaps the cords take on more significant roles in processing as the animals grow as our data largely involved studies of late juveniles. However, the characterization of the rest of the proboscis representing a peripheral nervous separated from a central nervous system is not well supported. Our transgene data supports extensive release throughout the plexus and may suggest that information processing occurs throughout the plexus of the animal. The broad dispersal of many neurons, characterized by peptidergic and classical transmitters, particularly in the proboscis and collar, also suggests that signal propagation occurs through tiling in a manner that has been proposed to represent ancestral nervous system function (Jékely 2021), and the characterization of the animal as having a "skin brain" may be the best analogy (Holland, 2003). Whether these varicosities represent true synapses or regions of volumetric release will require more detailed analysis with EM.

In conclusion, these data further build on existing data from classical studies in demonstrating that hemichordates do not share many organizational principles of the canonical centralized nervous systems of the main models that we study in neurobiology. This study in enteropneusts demonstrates that we have much to discover by sampling a far more diverse array of neural systems representing the rich biodiversity of the marine environment. Our molecular characterization does not reveal cryptic similarities with chordates that were not apparent from previous descriptive work. Yet, despite these profound differences in neural architectures, the early ectodermal patterning that establishes the contrasting neural systems of vertebrates and hemichordates is highly conserved (Lowe et al 2003, Pani et al 2012, Yao et al 2016). This work further develops the counterintuitive observation that regulatory conservation between distantly related groups has seemingly not restricted morphological diversification to a specific neural conformation over macroevolutionary time frames. We are far from understanding the link between gene regulatory conservation and nervous system evolution, and only by broadening our molecular scope into biodiversity are we likely to be able to recognize cryptic links between

908 morphological and molecular evolution that will allow us to address these important but difficult
909 questions of nervous system origins.

910 Materials and Methods

911 Animal collection and embryo culture

912 Adult worms were collected in the months of May and September during the *S. kowalevskii* breeding
913 seasons in Waquoit Bay, MA., and maintained in flow-through sea tables at the Marine Biological
914 Laboratory in Woods Hole, MA. Spawning fertilization and embryo culture followed protocols developed
915 by Colwin and Colwin (1950, 1962) with updated methods (Lowe et al., 2004).
916

917 Cloning of orthologs

918 *S. kowalevskii* homologs of vertebrate genes were identified in an EST library screen (Freeman et al.,
919 2008). See Supplemental Table for NIH accession numbers.
920

921 *In situ* hybridization

922 Whole mount *in situ* hybridization on juveniles was carried out using an established lab protocol (Lowe et
923 al., 2004). Embryos were kept in 5mL glass vials for all steps until the colorimetric reaction performed in
924 6 well tissue culture plates. Proteinase K treatment was carried out at 10µg/mL in PBTw for 15min at
925 room temperature (RT). Acetic anhydride treatment at 250µM for 5min at RT followed by a 500µM
926 treatment for 5 min at RT. *In situs* for experimental embryos were stained using 1.6µL:2.7µL ratio of 5-
927 Bromo-4-chloro-3-indolyl phosphate**:** nitro-blue tetrazolium chloride and stopped with 3x5 minute rinses
928 at RT in 1XMAB. Some samples were further cleared by rinsing 2×5 min in MeOH and cleared with a
929 2:1 ratio of benzyl benzoate: benzyl alcohol (BBBA) before imaging on a Zeiss Axioimager.

930

931 Whole mount *in situ* hybridizations on adults up to four gill slits utilized the same protocol as embryos
932 with minor modifications: Samples were permeablized for 15-20 minutes at room temperature in
933 Proteinase K diluted 1:7,500 in 1X PBST to increase probe penetration and staining in deeper tissues. The
934 proboscis coelom and gut were punctured with a tungsten needle or scalpel blade to reduce probe trapping
935 and increase penetration. For adult whole mount *in situ* hybridization, samples were dissected using a
936 scalpel or scissors to reduce probe trapping and increase staining of deeper tissues. The whole mount *in*
937 *situ* hybridization protocol was modified for adults by utilizing either large glass vials or 15 mL tubes and
938 performing at least two more washes than embryos for all steps.

939

940 *In situ* hybridization on tissue sections was based on the protocol for embryos with technical
941 modifications for slides. Fixed adults were dissected into pieces no more than 3 cm in length and
942 cryoprotected in an increasing concentration gradient of sucrose in fixation buffer up to 20% sucrose at
943 room temperature and allowed to equilibrate overnight at 4ºC. Samples were then placed in 20% sucrose
944 in fixation buffer diluted 2:1 in OCT media (Fisher) and allowed to equilibrate at room temperature with
945 gentle agitation. Fixation buffer was utilized instead of 1X PBS to reduce tissue swelling and sectioning
946 artifacts. Samples were embedded in plastic molds, chilled on dry ice, and stored indefinitely at -80ºC.
947 Frozen blocks were sectioned at 16-25 mm using a Leica cryostat with a cutting temperature between -25
948 and -30ºC. Sections were collected on Superfrost Plus slides (Fisher), allowed to dry for at least 20
949 minutes, and either processed for *in situ* hybridizations or immunofluorescence immediately or stored at -
950 80ºC. Sections were permeablized with 0.2% Triton X-100 in 1X PBST for 20 minutes rather than with
951 Proteinase K, and all washes were performed in upright slide mailers. For hybridization, sections were
952 covered using plastic Hybrislip cover slips (Grace Technologies) and placed facing up in horizontal slide
953 mailers with a Kimwipe or filter paper soaked in hybridization solution to prevent the slide from drying.
954 Slide mailers were sealed using tape, placed in chambers constructed from empty pipette tip boxes, and
955 hybridized overnight in an oven at 60ºC. For blocking and antibody steps, sections were outlined using a

956 hydrophobic marker, and incubations were performed on slides placed horizontally in humidified
957 chambers at room temperature or at 4ºC overnight. Different probes were hybridized in separate
958 chambers.
959
960 Hybridization Chain Reaction (HCR) in situ hybridization: DNA probe sets were generated and ordered
961 from Molecular Instruments, Inc. using the full RNA sequence from GeneBank accession numbers TH
962 (XM_006813504.1), DAT (NM_001168055), VGLUT (XM_002739644), GAD (XM_002740628),
963 achatin (XM_002732101.2), CCK (XM_002738068.2), and orexin (XM_002734948.2). 11-33 probe sets
964 were generated for each gene, and DNA oligo pools were resuspended to a final concentration of
965 1μmol/μl in 50 mM Tris buffer, pH 7.5. HCR amplifiers, B1-Alexa Fluor-546, B2-Alexa Fluor-488, and
966 B3-Alexa Fluor-647, were ordered from Molecular Instruments, Inc. HCR version 3.0 protocol (Choi et
967 al., 2018), and a protocol from Nipam Patels lab.
968

969 **Immunohistochemistry**

970 Juveniles were reared and fixed as previously described (Lowe et al., 2004) Briefly, embryos were fixed
971 for 30 min at room temperature in fixation buffer (3.7% formaldehyde, 0.1 M MOPS pH 7.5, 0.5 M NaCl,
972 2 mM EGTA pH 8.0, 1 mM MgCl2, 1X PBS), and subsequently stored in ethanol at −20 °C. For anti-
973 GABA, we used 3.7% formaldehyde and 0.3% glutaraldehyde. For antibody staining, embryos were
974 rehydrated into 1x PBS +0.1% Triton X-100 (PBSTr), rinsed 3 × 10 min in PBSTr, and placed into a
975 blocking solution of 1x PBS +0.1% Tween 20 (PBT) +5% goat serum for 2 h at room temperature.
976 Embryos were incubated in PBT with either anti-GFP (Life Technologies, #A-6455), anti-FMRFamide
977 (Immunostar, #20091), anti-5HT (Sigma, S5545), or anti-GABA (Sigma, A2052) at a 1:500 dilution
978 overnight at 4 °C. After primary antibody incubation, embryos were washed 4 × 30 min in PBSTr, and
979 then incubated for 4 h at room temperature with secondary antibody (Alexa-Fluor 488 goat anti-rabbit
980 IgG, ThermoFisher #A-11008) diluted 1:500 in blocking solution. Samples were then washed 4 × 30 min

981 in PBSTr and cleared into 80% glycerol. Some samples were further cleared by rinsing 2 × 5 min in
982 MeOH and cleared with a 2:1 ratio of benzyl benzoate: benzyl alcohol (BBBA). Images were captured on
983 a ZEIS LSM 700 confocal microscope with 20× and 40× objectives using the Zen software package (Carl
984 Zeiss).
985
986 Immunofluorescence on adult tissue sections was performed as described previously with minor
987 modifications. Sections were outlined with a hydrophobic marker, and wash steps were performed in an
988 upright slide mailer. Blocking and antibody incubation steps were performed on slides placed horizontally
989 in humidified chambers at room temperature. Primary antibody incubations were: 1E11, 1:3 (gift of
990 Robert Burke); rabbit anti-serotonin, 1:250 (Sigma S5545); mouse anti-FMRFamide, 1:600 (Immunostar
991 #20091). Secondary antibody (Molecular Probes) dilutions were: Alexa Fluor 488 goat anti-mouse or
992 rabbit, 1:500; Alexa Fluor 546 goat anti-mouse or rabbit, 1:1000; Alexa Fluor goat anti-mouse or rabbit
993 647, 1:250. Imaging was performed using a Zeiss LSM700 confocal microscope with Zeiss Zen software,
994 an Olympus FV1000 confocal microscope with Olympus software, or a Zeiss Axioimager.Z1 compound
995 microscope or Discovery.V12 stereomicroscope with an Axiocam MRm camera and Zeiss Axiovision
996 software.
997

998 **Transgenes**

999 5-8kb of putative promoters and enhancers sequence directly upstream of the start codon for genes TH
1000 (5kb, XM_006813504.1) and synapsin (8kb, XP_006820290.1) were cloned into a reporter plasmid based
1001 designed for developmental studies in Lampreys (Parker et al., 2014) containing I-SceI meganuclease
1002 restriction sites, upstream of an eGFP coding sequence and a SV40 late polyadenylation signal sequence
1003 using Gibson assembly (Gibson et al., 2009; Parker et al., 2014) and previously published (Minor et al.,
1004 2019). Full regulatory sequence for each transgene is included in Supplementary Table 1. Injection
1005 mixtures contained 10µl restriction digest including 5 units of I-SceI enzyme (NEB), 1µl CutSmart buffer,

1006 and 130ng of reporter plasmid, final concentration 13ng/µl. The mixture was incubated at 37 °C for 40
1007 min and injected into embryos between 4-9 min post fertilization as previously described (Minor et al.,
1008 2019). To visualize regions of transmitter release, the mouse synaptophysin-mRuby fusion protein was
1009 cloned into the generated synapsin:eGFP transgene from AAV-FLExloxP-mGFP-2A-synaptophysin-
1010 mRuby (Addgene Plasmid# 71760) plasmid vector courtesy of Liqun Luo (Beier et al., 2015) to generate
1011 the synapsin:mGFP-2A-(mouse)synaptophysin-mRuby transgene. Vector inset sequence and primers used
1012 for the generation of these plasmids are listed in Supplementary Table 1. Reconstruction of neural
1013 projections for a subset of neurons were generated using the 3D Visualization-Assisted Analysis (Vaa3D)
1014 software suite (Peng et al., 2014).
1015

1016 Acknowledgements
1017 We would like to thank the Staff of the Marine Biological Laboratory for hosting us and their assistance
1018 in pursuit of our research. The Waquoit National Estuarine Research Reserve for allowing access to our
1019 collection site. Jim Mcilvain from Zeiss for assistance in microscopy, Robb Krumlauf and Hugo Parker
1020 for providing the vector for our transgenics. Thurston Lacalli for his guidance and discussions on the
1021 evolutionary implications of this work, and Laurent Formery for his editorial input. This work was
1022 supported by an NSF grant (1656628) to CJL**.**
1023

1024 Figure Legends

1025 **Figure 1: Pan-neural marker, *elav*, expression**

1026 (A) An illustration representing the transverse and sagittal sections taken along the adult body. (B, C)
1027 Transverse sections at the base of the proboscis show circumferential *elav* expression, with most
1028 extensive expression at the far proboscis base. (D-F) Anterior collar sections with dorsal to the right. (E)
1029 Higher magnification of the inset from D focused on the proboscis stem. *elav* staining in both the

1030 ectoderm and pharyngeal epithelium (PhEp) and in the anterior collar ring (ACR). (G-I) sections from the
1031 posterior collar with I showing a high magnification of inset from (H). (J) Section at the posterior trunk
1032 with expression in both dorsal (DNC) and ventral cords (VNC). (K-M) Sagittal sections from proboscis to
1033 anterior trunk. (K) Left of the midline, (L) on the midline showing the dorsal cord through the collar, and
1034 (M) to the right of the midline. (N, O) Late juvenile stage, whole mount. (N) Lateral view and (O), dorsal
1035 view of proboscis and collar. (P) *Elav* expression in dissected adult trunk ventral ectoderm showing the
1036 ventral cord. (Q) Whole mount adult proboscis dorsal view. (R) Dorsal view of adult anterior trunk. (S)
1037 Dorsal view of posterior trunk. Scale bars equal 250 µm, except in P-S 500 µm.
1038

1039 **Figure 2: Expression of neurotransmitter markers**

1040 Gene expression in juvenile and adult tissue for components of neurotransmitter synthesis and transport
1041 genes. (A-B') *Tyrosine Hydroxylase*. White arrowheads indicate expression at the base of the proboscis,
1042 open arrowhead at the tip of the collar, and black arrowhead at the anterior trunk. (A) Expression in early
1043 juvenile lateral view, (A') late juvenile lateral view. (B) Whole mount expression in adult proboscis, (B')
1044 lateral view of adult collar and base of proboscis. (C-C''') coexpression of tyrosine hydroxylase and
1045 dopamine transporter in (C), early juvenile lateral view (AP – anterior proboscis, PB-proboscis base, and
1046 AC – anterior collar) with (C') a high magnification of the anterior proboscis, and (C"), a high
1047 magnification of the base of the proboscis. (C''') Proboscis and collar of late juvenile. (D) Lateral view of
1048 an early juvenile showing expression of *tryptophan hydroxylase*. (E,E') Expression of *histidine*
1049 *decarboxylase* (white arrow indicates base of proboscis) in (E), early juvenile, and (E'), late juvenile. (F-
1050 F'') Expression of *vesicular glutamate transporter* in (F), early juvenile, lateral view with lower inset
1051 showing dorsal view of the collar and anterior trunk, (F'), dorsal view of later juvenile of the proboscis
1052 and collar and (F"), dorsal view of the trunk of a late juvenile. (G-H') Expression of *glutamate*
1053 *decarboxylase* in (G), early juvenile and (G'), late juvenile in lateral view, (H), whole mount of adult tip
1054 of the proboscis, (H'), dorsal view of the adult collar and posterior proboscis. (I) Lateral and (I') dorsal

1055 view of *vesicular GABA transporter* expression in early juvenile. Scale bars are 100 µm in early
1056 juveniles, 200 µm in late juveniles, and 500 µm in adults.
1057

1058 **Figure 3: Expression of neuropeptide markers**

1059 Gene expression in early and late juveniles for components of neuropeptide signaling including synthesis
1060 and transport genes. (A-C’’’) Co-expression of three neuropeptide synthesis genes in early juveniles in
1061 (A) lateral and (B) dorsal views. (C-C’’’) Zoomed-in panels of the dorsal proboscis. (D) *Proprotein*
1062 *convertase 2* expression in early juvenile lateral view, and (D’), expression in late juvenile, both in lateral
1063 view. (E) Expression of *glutaminyl-peptide cyclohydrolase* in P, early juvenile, and (E’), late juvenile.
1064 (F)Vasotocin expression in early and (F’) late juvenile. (G) Expression of VLamide (VIG) in early and
1065 (G’) late juvenile, and with inset showing a dorsal view (G) and lateral view (G’). (H) Expression of
1066 Luqin in (H), early juvenile and (H’), late juvenile. (I) Gonadotropin-Releasing Hormone expression in
1067 early and late (I’) juvenile. Zoomed-in inset (I) shows proximal axonal projections from neurons in the
1068 trunk. (I’) Dorsal view of late juvenile. (J) Expression of neuropeptide WFMRFamide in (J), early
1069 juvenile, and (J’), late juvenile. (K) Expression of the neuropeptide NNFamide in (K), early juvenile, and
1070 (K’), late juvenile, both in lateral view. (L) Corticotrophin-releasing hormone expression in early and late
1071 juvenile (L’), inset shows expression at the heart-kidney complex at the proboscis base. (M) *Orexin*
1072 expression in (M), early juvenile and (M’) late juvenile, both lateral views. (N) Calcitonin (CalC)
1073 expression in early juvenile, with inset showing proximal axon projections at the proboscis, and late
1074 juvenile (N’), with inset showing expression using RNA-based probe. (O)Thyrotropin-releasing hormone
1075 (TRH) expression in (O), early juvenile with the dorsal view of the proboscis in the inset, and (O’) late
1076 juvenile. (P) *Achatin* expression in (P), early juvenile and (P’) late juvenile, both lateral views, with only
1077 the proboscis and collar shown in (P’). (Q) Cholecystokinin expression in early and (Q’) late juvenile,
1078 lateral views. (R) Co-expression of the neuropeptides NNFamide, TRH, and WFMRFamide in early and

1079 (R’’) late juvenile, with insets (R’, R’’’) showing zoomed-in proboscis base. Scale bars are 100 µm in
1080 early juveniles and 200 µm in late juveniles.
1081

1082 **Figure 4: Neural plexus organization**

1083 Visualization of the neural plexus in fixed and live tissue using an anti-synaptotagmin antibody (A-I), DiI
1084 (J-M), and Neo O (N). Juveniles are imaged in whole mount, and adult ectoderm by flat mount following
1085 dissection and imaging from the basal surface. (A) Maximum projection of a late juvenile stained for
1086 synaptotagmin (1E11), lateral view. (B) high magnification section of adult ectoderm at the base of the
1087 proboscis. (C) Illustration showing the performed excision of the posterior proboscis ectoderm from an
1088 adult animal. (D-I) Expression of synaptotagmin in dissected adult ectoderm in different regions of the
1089 body: (D) dorsal proboscis showing dorsal cord, (E) posterior proboscis base dissected as shown in (C),
1090 (F) anterior region of the proboscis base, (G) posterior region of the proboscis base, (H) the anterior
1091 collar, and (I) the dorsal trunk. (J-M) Lipophilic dye (DiI) injections into adult fixed tissue reveals dye
1092 diffusion across the adult plexus in (J) and (K), and neurite cell morphology in (L) and (M). (N) Live
1093 neural marker, NeuO, showing similar puncta along neurites seen in fixed tissue in (L) and (M). Scale
1094 bars represent 250 µm in A,D,E,I-K and 25 µm in B,F-H,L-N.
1095

1096 **Figure 5: Serotonergic nervous system**

1097 Investigation of the serotonergic nervous system in juveniles (A-E) and adults (F-Q) using anti-5HT. (A)
1098 Maximum projection of a late juvenile lateral view. (B) High magnification of bipolar neurons with a
1099 sensory cilium projecting towards the apical region of the epithelium and a single neurite projecting
1100 basally into the neural plexus. (C-E) High magnification images from panels shown in (A): (C) posterior
1101 proboscis, (D) collar, and (E) trunk. Images are oriented in an anterior (left)-to-posterior(right) and a

1102 dorsal (up)-to-ventral(down) direction. (F-J) Adult ectoderm in the proboscis; (F) mid proboscis, (G, H)
1103 base of the proboscis double labelled with synaptotagmin, and the same specimen as in Fig 3E. (I) collar,
1104 and (J) trunk. (K) An illustration showing the sagittal sections carried out in adult tissues: All sections
1105 oriented with dorsal at the top of the panel with phalloidin labelled in purple, 5HT in white, and DAPI in
1106 blue. (L) proboscis, (M) mid-collar, (N) higher magnification of the dorsal collar cord, (O) anterior trunk,
1107 and (P) and (Q) showing the tail. Scale bars represent 500 µm in F,I,J,L,M, O-Q, 200 µm in A,G,N, 20
1108 µm in B-E,H.
1109

1110 **Figure 6: GABAergic and FMRFamidergic nervous system**

1111 Distribution of GABAergic and peptidergic neurons in juveniles and adults using anti-GABA and anti-
1112 FMRFamide polyclonal antibodies. (A-Aiii) distribution of GABA in juveniles. (A) Maximum projection
1113 of a late juvenile (Black arrows in A point to the ring of GABA neurons at the anterior collar), and higher
1114 magnification of the same individual at 3 different regions: (Ai) anterior proboscis, (Aii) anterior dorsal
1115 trunk (arrows indicating the dendrites projecting to the outer epithelium of both the ectoderm and
1116 endoderm), and (Aiii) endodermal plexus in the pharyngeal gut of the anterior trunk, with neurites
1117 projecting around the gill slits (GS). (B-E) Dissected adult tissue at (B) the proboscis base, (C) collar, (D)
1118 gill slits at the trunk, and (E) dissected dorsal collar cord. (F) Maximum projection of a late juvenile
1119 labeled with anti-FMRF-amide, panels show the position of the subsequent high magnification images; Fi
1120 anterior collar and proboscis stem, (Fii) ventral trunk/ventral cord, and (Fiii) postanal tail. (G) Adult
1121 proboscis plexus. Scale bars are 100 µm, except 20 µm in panels Ai-Aiii, and Fi-Fiii.
1122

1123 **Figure 7: Neural cell morphology and neurite projection using a synapsin:GFP transgene**

1124 (A, B) Maximum projection of two representative synapsin:eGFP animals using 8kb regulatory sequence
1125 upstream of the synapsin I gene to drive expression of cytoplasmic eGFP. (Ai-Aiv) and (Bi-Bii) are high
1126 magnification panels for each juvenile revealing detailed cellular morphology and neurite projections.
1127 (Ai) The anterior proboscis plexus, red arrows point to varicosities along neurites. (Aii) The dorsal cord
1128 connecting the proboscis and collar, red arrow points to a single axon and green arrow points to a
1129 bifurcated axon from neurons projecting into the cord. (Aiii) Dorsal posterior collar, neurons projecting
1130 anteriorly along the dorsal collar cord, with red arrows indicating projecting axons. (Aiv) Postanal tail
1131 with detailed cellular morphology of neurons projecting anteriorly. (Bi) Anterior proboscis showing
1132 sensory cells projecting into the ectodermal plexus. (Bii) Pair of sensory cells in the apical tuft region that
1133 appear to project locally to interneuron in the plexus, indicated by red arrows. (Biii) Mid-proboscis with
1134 anteriorly projecting sensory neurons. (C) Projection trajectories from neurons in the dorsal posterior
1135 collar, right above the first gill slit, projecting anteriorly towards the dorsal proboscis base. (D-G)
1136 Representative neural cell type polarities across different animals. Scale bars in A,B represent 100 µm
1137 and 20 µm in Ai-G.
1138

1139 **Figure 8: Localization of synaptophysin along axons at varicosities**

1140 A, E Synapsin:mGFP—T2A—(mouse)Synaptophysin-mRuby expression from two representative
1141 animals using 8kb regulatory sequence upstream of the synapsin I gene to drive expression of mGFP and
1142 the mouse synaptophysin-mRuby fusion protein cleaved off by the self-cleaving enzyme sequence, T2A.
1143 Mosaic expression of Transgene in 2 representative animals Synaptophysin-mRuby (SYP-mRuby)
1144 expression is shown in green channel, synapsin:eGFP (SYN:eGFP) expression in magenta, and nuclear
1145 stain with DAPI in blue. (A) Transgene expression in the proboscis neural plexus with higher
1146 magnification in (B) anterior proboscis, (C) posterior proboscis base, and (D) dorsal posterior ectoderm.
1147 (E) Second animal showing a single neuron expressing the transgene, dorsal view. The cell body is in the
1148 tail and projects into the proboscis. (F-H) Higher magnification panels along the length neuron: (F) neural

1149 cell body, (G) mid-axon at the dorsal posterior collar, (H) axon terminal at the mid-proboscis. G', H', and
1150 H'' are higher magnification images to show SYP-mRuby puncta along the axon, H' is the axon terminal.
1151 Scale bars in A,E are 100 µm and 20µm in B-D, and F-H'.
1152

1153 **Figure 9: TH:GFP transgene**

1154 (A) Maximum projection of a TH:eGFP representative animal using 5KB regulatory sequence upstream
1155 of the TH gene to drive expression of cytoplasmic eGFP. (B-D) Higher magnification images at (B)
1156 anterior proboscis, (C) ventral posterior proboscis, and (D) ventral collar. (E) Proboscis ectoderm from a
1157 different animal showing detailed cellular morphology of TH+ neurons. (F-K') Manually traced axons
1158 from sensory neurons that project posteriorly in the proboscis (F, F'), collar neurons that project
1159 anteriorly towards the proboscis (G-I'), and proboscis base neurons that project anteriorly towards the
1160 proboscis tip (J-K'). Scale bars in A represent 100 µm, 50 µm in F-K, and 20 µm in B-E and F'-K'.
1161

1162 Supplemental Figure Legends
1163

1164 **Supplemental Table:**

1165 (A) NIH EST accession numbers for *S. kowalevskii* homologs of vertebrate genes identified in an EST
1166 library screen (Freeman et al., 2008). (B) Gene sequence and accession number used to generate the HCR
1167 hairpins. (C) Primer sequence used to generate fragments for transgene listen in D. (D) Transgene name
1168 and sequence used in this study as well as the gene accession number.
1169

1170 **Supplemental Movie 1:**

1171 A Z-stack along the trunk of an adult clearly showing the layered nature of the plexus against the
1172 synaptotagmin 1 (1E11) antibody.
1173

1174 **Supplemental Movie 2:**

1175 A Z-stack along the collar and trunk of a 3GS juvenile. The 5HT antibody clearly shows the serotonergic
1176 nervous system composed of many sensory neurons at the collar and trunk with a basipethelial neural
1177 plexus.
1178

1179 References

1180 Ajayi, A., Withyachumnarnkul, B., 2013. Presence and distribution of FMRFamide-like
1181 immunoreactivity in the sea cucumber Holothuria scabra (Jaeger, 1833). Zoomorphology 132, 285-300.
1182 Antzoulatos, E.G., Byrne, J.H., 2004. Learning insights transmitted by glutamate. Trends Neurosci 27,
1183 555-560.
1184 Arendt, D., Nubler-Jung, K., 1994. Inversion of dorsoventral axis? Nature 371, 26.
1185 Arendt, D., Nubler-Jung, K., 1996. Common ground plans in early brain development in mice and flies.
1186 Bioessays 18, 255-259.
1187 Aronowicz, J., Lowe, C.J., 2006. Hox gene expression in the hemichordate Saccoglossus kowalevskii and
1188 the evolution of deuterostome nervous systems. Integrative and comparative biology 46, 890-901.
1189 Bateson, W., 1885. Later stages in the development of Balanoglossus Kowalevskii with a suggestion as to
1190 the affinities of the Enteropneusta. Quarterly Journal of Microscopical Science 25, 81-128.
1191 Bateson, W., 1886. The ancestry of the chordata. Quarterly Journal of Microscopical Science 26, 535-
1192 571.
1193 Beier, K.T., Steinberg, E.E., DeLoach, K.E., Xie, S., Miyamichi, K., Schwarz, L., Gao, X.J., Kremer, E.J.,
1194 Malenka, R.C., Luo, L., 2015. Circuit Architecture of VTA Dopamine Neurons Revealed by Systematic
1195 Input-Output Mapping. Cell 162, 622-634.
1196 Bromham, L.D., Degnan, B.M., 1999. Hemichordates and deuterostome evolution: robust molecular
1197 phylogenetic support for a hemichordate + echinoderm clade. Evolution & development 1, 166-171.
1198 Brown, F.D., Prendergast, A., Swalla, B.J., 2008. Man is but a worm: chordate origins. Genesis 46, 605-
1199 613.
1200 Bullock, T.H., 1940. The functional organisation of the nervous system of the Enteropneusta. Biological
1201 Bulletin 79, 91.
1202 Bullock, T.H., 1944. The giant nerve fibre system in Balanoglossids. J. Comp. Neurol. 80, 355.
1203 Bullock, T.H., 1945. The anatomical organization of the nervous system of enteropneusta. Quart. J.
1204 Microscrop. Sci. 86, 55-112.
1205 Bullock, T.H., Horridge, G.A., 1965. Structure and function in the nervous systems of invertebrates. W.
1206 H. Freeman, San Francisco.
1207 Burbach, J.P., 2011. What are neuropeptides? Methods Mol Biol 789, 1-36.

1208 Busby, W.H., Jr., Quackenbush, G.E., Humm, J., Youngblood, W.W., Kizer, J.S., 1987. An enzyme(s)
1209 that converts glutaminyl-peptides into pyroglutamyl-peptides. Presence in pituitary, brain, adrenal
1210 medulla, and lymphocytes. J Biol Chem 262, 8532-8536.
1211 Byrne, M., Nakajima, Y., Chee, F.C., Burke, R.D., 2007. Apical organs in echinoderm larvae: insights
1212 into larval evolution in the Ambulacraria. Evolution & development 9, 432-445.
1213 Cameron, C.B., Garey, J.R., Swalla, B.J., 2000. Evolution of the chordate body plan: new insights from
1214 phylogenetic analyses of deuterostome phyla. Proc Natl Acad Sci U S A 97, 4469-4474.
1215 Cannon, J.T., Kocot, K.M., Waits, D.S., Weese, D.A., Swalla, B.J., Santos, S.R., Halanych, K.M., 2014.
1216 Phylogenomic resolution of the hemichordate and echinoderm clade. Curr Biol 24, 2827-2832.
1217 Choi, H.M.T., Schwarzkopf, M., Fornace, M.E., Acharya, A., Artavanis, G., Stegmaier, J., Cunha, A.,
1218 Pierce, N.A., 2018. Third-generation in situ hybridization chain reaction: multiplexed, quantitative,
1219 sensitive, versatile, robust. Development 145.
1220 Cobb, J.L., Pentreath, V.W., 1977. Anatomical studies of simple invertebrate synapses utilizing stage
1221 rotation election microscopy and densitometry. Tissue Cell 9, 125-135.
1222 Cobb, J.L., Pentreath, V.W., 1978. Comparison of the morphology of synapses in invertebrate and
1223 vertebrate nervous systems: analysis of the significance of the anatomical differences and interpretation of
1224 the morphological specializations. Prog Neurobiol 10, 231-252.
1225 Cunningham, D., Casey, E.S., 2014. Spatiotemporal development of the embryonic nervous system of
1226 Saccoglossus kowalevskii. Dev Biol 386, 252-263.
1227 Danbolt, N.C., 2001. Glutamate uptake. Prog Neurobiol 65, 1-105.
1228 Darras, S., Fritzenwanker, J.H., Uhlinger, K.R., Farrelly, E., Pani, A.M., Hurley, I.A., Norris, R.P.,
1229 Osovitz, M., Terasaki, M., Wu, M., Aronowicz, J., Kirschner, M., Gerhart, J.C., Lowe, C.J., 2018.
1230 Anteroposterior axis patterning by early canonical Wnt signaling during hemichordate development.
1231 PLoS Biol 16, e2003698.
1232 Dawydoff, C., 1948. Classe des Entéropneustes., in: Grassé, P.P. (Ed.), Traité de Zoologie, Paris:
1233 Libraries de l'Academie de Médecine, pp. 369-453
1234 De Camilli, P., Harris, S.M., Jr., Huttner, W.B., Greengard, P., 1983. Synapsin I (Protein I), a nerve
1235 terminal-specific phosphoprotein. II. Its specific association with synaptic vesicles demonstrated by
1236 immunocytochemistry in agarose-embedded synaptosomes. J Cell Biol 96, 1355-1373.
1237 de Castro, F., 1950. Die Normale Histologie des Peripheren Vegetativen Nervensystems: Das Synapsen-
1238 Problem Anatomisch-experimentelle UntersuchungAnatomisch-experimentelle Untersuchung. Julius
1239 Springer.
1240 De Robertis, E.M., 2008. Evo-devo: variations on ancestral themes. Cell 132, 185-195.
1241 De Robertis, E.M., Sasai, Y., 1996. A common plan for dorsoventral patterning in Bilateria. Nature 380,
1242 37-40.
1243 Denes, A.S., Jekely, G., Steinmetz, P.R., Raible, F., Snyman, H., Prud'homme, B., Ferrier, D.E.,
1244 Balavoine, G., Arendt, D., 2007. Molecular architecture of annelid nerve cord supports common origin of
1245 nervous system centralization in bilateria. Cell 129, 277-288.
1246 Descarries, L., Berube-Carriere, N., Riad, M., Bo, G.D., Mendez, J.A., Trudeau, L.E., 2008. Glutamate in
1247 dopamine neurons: synaptic versus diffuse transmission. Brain Res Rev 58, 290-302.
1248 Descarries, L., Gisiger, V., Steriade, M., 1997. Diffuse transmission by acetylcholine in the CNS. Prog
1249 Neurobiol 53, 603-625.
1250 Descarries, L., Mechawar, N., 2000. Ultrastructural evidence for diffuse transmission by monoamine and
1251 acetylcholine neurons of the central nervous system. Prog Brain Res 125, 27-47.
1252 Diaz-Miranda, L., Blanco, R.E., Garcia-Arraras, J.E., 1995. Localization of the heptapeptide
1253 GFSKLYFamide in the sea cucumber Holothuria glaberrima (Echinodermata): a light and electron
1254 microscopic study. J Comp Neurol 352, 626-640.
1255 Dilly, P.N., 1969. The nerve fibres in the basement membrane and related structures in Saccoglossus
1256 horsti (Enteropneusta). Z Zellforsch Mikrosk Anat 97, 69-83.
1257 Dilly, P.N., Welsch, U., Storch, V., 1970. The structure of the nerve fiber layer and neurocord in the
1258 enteropneusts. Z. Zellforsch. Mikrosk. Anat. 103, 129-148.

1259 Elphick, M.R., 2010. NG peptides: a novel family of neurophysin-associated neuropeptides. Gene 458,
1260 20-26.
1261 Elphick, M.R., Mirabeau, O., 2014. The Evolution and Variety of RFamide-Type Neuropeptides: Insights
1262 from Deuterostomian Invertebrates. Front Endocrinol (Lausanne) 5, 93.
1263 Elphick, M.R., Mirabeau, O., Larhammar, D., 2018. Evolution of neuropeptide signalling systems. J Exp
1264 Biol 221.
1265 Er, J.C., Leong, C., Teoh, C.L., Yuan, Q., Merchant, P., Dunn, M., Sulzer, D., Sames, D., Bhinge, A.,
1266 Kim, D., Kim, S.M., Yoon, M.H., Stanton, L.W., Je, S.H., Yun, S.W., Chang, Y.T., 2015. NeuO: a
1267 fluorescent chemical probe for live neuron labeling. Angew Chem Int Ed Engl 54, 2442-2446.
1268 Fischer, W.H., Spiess, J., 1987. Identification of a mammalian glutaminyl cyclase converting glutaminyl
1269 into pyroglutamyl peptides. Proc Natl Acad Sci U S A 84, 3628-3632.
1270 Flood, P.R., 1966. A peculiar mode of muscular innervation in Amphioxus. Light and electron
1271 microscopic studies of the so-called ventral roots. J Comp Neurol 126, 181-217.
1272 Fonnum, F., 1984. Glutamate: a neurotransmitter in mammalian brain. J Neurochem 42, 1-11.
1273 Furlong, R.F., Holland, P.W., 2002. Bayesian phylogenetic analysis supports monophyly of ambulacraria
1274 and of cyclostomes. Zoolog Sci 19, 593-599.
1275 Garstang, W., 1894. Preliminary note on a new theory of the phylogeny of the chordata. Zool. Anzeiger
1276 22, 122-125.
1277 Garstang, W., 1928. The morphology of the Tunicata. Quart J. Miscroscop. Sci. 72, 51-189.
1278 Geoffroy-St. Hilaire, E., 1822. Considérations générales sur les vertebrés. Mem. HIst. Nat. 9, 89-119.
1279 Gerschenfeld, H.M., 1973. Chemical transmission in invertebrate central nervous systems and
1280 neuromuscular junctions. Physiol Rev 53, 1-119.
1281 Gibson, D.G., Young, L., Chuang, R.Y., Venter, J.C., Hutchison, C.A., 3rd, Smith, H.O., 2009.
1282 Enzymatic assembly of DNA molecules up to several hundred kilobases. Nat Methods 6, 343-345.
1283 Gonzalez, P., Uhlinger, K.R., Lowe, C.J., 2017. The Adult Body Plan of Indirect Developing
1284 Hemichordates Develops by Adding a Hox-Patterned Trunk to an Anterior Larval Territory. Curr Biol 27,
1285 87-95.
1286 Greer, J.B., Khuri, S., Fieber, L.A., 2017. Phylogenetic analysis of ionotropic L-glutamate receptor genes
1287 in the Bilateria, with special notes on Aplysia californica. BMC Evol Biol 17, 11.
1288 Hejnol, A., Lowe, C.J., 2015. Embracing the comparative approach: how robust phylogenies and broader
1289 developmental sampling impacts the understanding of nervous system evolution. Philos Trans R Soc
1290 Lond B Biol Sci 370.
1291 Hess, W.N., 1937. The nervous system of Dolichoglossus kowalevskyi. Journal of Experimental Zoology
1292 79, 1-11.
1293 Hewes, R.S., Taghert, P.H., 2001. Neuropeptides and neuropeptide receptors in the Drosophila
1294 melanogaster genome. Genome Res 11, 1126-1142.
1295 Hirth, F., 2010. On the origin and evolution of the tripartite brain. Brain Behav Evol 76, 3-10.
1296 Hirth, F., Reichert, H., 1999. Conserved genetic programs in insect and mammalian brain development.
1297 Bioessays 21, 677-684.
1298 Hoekstra, L.A., Moroz, L.L., Heyland, A., 2012. Novel insights into the echinoderm nervous system from
1299 histaminergic and FMRFaminergic-like cells in the sea cucumber Leptosynapta clarki. PLoS One 7,
1300 e44220.
1301 Holland, L.Z., 2015. Evolution of basal deuterostome nervous systems. J Exp Biol 218, 637-645.
1302 Holland, N.D., 2003. Early central nervous system evolution: an era of skin brains? Nat Rev Neurosci 4,
1303 617-627.
1304 Holland, N.D., Holland, L.Z., Holland, P.W., 2015. Scenarios for the making of vertebrates. Nature 520,
1305 450-455.
1306 Horst, C.J.v.d., 1939. Hemichordata. Akademische Verlagsgesellschaft m.b.H., Leipzig.
1307 Hulett, R.E., Potter, D., Srivastava, M., 2020. Neural architecture and regeneration in the acoel Hofstenia
1308 miamia. Proceedings. Biological sciences / The Royal Society 287, 20201198.

1309 Huttner, W.B., Schiebler, W., Greengard, P., De Camilli, P., 1983. Synapsin I (protein I), a nerve
1310 terminal-specific phosphoprotein. III. Its association with synaptic vesicles studied in a highly purified
1311 synaptic vesicle preparation. J Cell Biol 96, 1374-1388.
1312 Hyman, L.H., 1955. The invertebrates, 1st ed. McGraw-Hill, New York,.
1313 Jackson, F.R., Newby, L.M., Kulkarni, S.J., 1990. Drosophila GABAergic systems: sequence and
1314 expression of glutamic acid decarboxylase. J Neurochem 54, 1068-1078.
1315 Jekely, G., 2013. Global view of the evolution and diversity of metazoan neuropeptide signaling. Proc
1316 Natl Acad Sci U S A 110, 8702-8707.
1317 Jekely, G., 2021. The chemical brain hypothesis for the origin of nervous systems. Philos Trans R Soc
1318 Lond B Biol Sci 376, 20190761.
1319 Kaul, S., Stach, T., 2010. Ontogeny of the collar cord: neurulation in the hemichordate Saccoglossus
1320 kowalevskii. J Morphol 271, 1240-1259.
1321 Kaul-Strehlow, S., Röttinger, E., 2015. Hemichordata, in: Wanninger, A. (Ed.), Evolutionary
1322 Developmental Biology of Invertebrates 6: Deuterostomia. Springer Vienna, Vienna, pp. 59-89.
1323 Kaul-Strehlow, S., Stach, T., 2013. A detailed description of the development of the hemichordate
1324 Saccoglossus kowalevskii using SEM, TEM, Histology and 3D-reconstructions. Frontiers in Zoology 10,
1325 1-31.
1326 Kaul-Strehlow, S., Urata, M., Minokawa, T., Stach, T., Wanninger, A., 2015. Neurogenesis in directly
1327 and indirectly developing enteropneusts: of nets and cords. Org Divers Evol 15, 405-422.
1328 Kaul-Strehlow, S., Urata, M., Praher, D., Wanninger, A., 2017. Neuronal patterning of the tubular collar
1329 cord is highly conserved among enteropneusts but dissimilar to the chordate neural tube. Sci Rep 7, 7003.
1330 Kinjo, A., Koito, T., Kawaguchi, S., Inoue, K., 2013. Evolutionary history of the GABA transporter
1331 (GAT) group revealed by marine invertebrate GAT-1. PLoS One 8, e82410.
1332 Knight-Jones, E., 1952. On the nervous system of Saccoglossus cambriensis (Enteropneusta). . Philos.
1333 Trans. R. Soc. Lond. B. Biol. Sci. 236, 315-354.
1334 Komai T. The homology of the" notochord" found in pterobranchs and enteropneusts. The American
1335 Naturalist. 1951 Jul 1;85(823):270-1.
1336 Kowalevsky, A., 1866. Anatomie des Balanoglossus. Mem Acad Imp Sci St Petersburg 7, 16.
1337 Krishnan, A., Almen, M.S., Fredriksson, R., Schioth, H.B., 2013. Remarkable similarities between the
1338 hemichordate (Saccoglossus kowalevskii) and vertebrate GPCR repertoire. Gene 526, 122-133.
1339 Lemaire LA, Cao C, Yoon PH, Long J, Levine M. The hypothalamus predates the origin of vertebrates.
1340 Science Advances. 2021 Apr 28;7(18):eabf7452.
1341 Lichtneckert, R., Reichert, H., 2005. Insights into the urbilaterian brain: conserved genetic patterning
1342 mechanisms in insect and vertebrate brain development. Heredity (Edinb) 94, 465-477.
1343 Lippens, S., Kremer, A., Borghgraef, P., Guerin, C.J., 2019. Serial block face-scanning electron
1344 microscopy for volume electron microscopy. Methods Cell Biol 152, 69-85.
1345 Lowe, C.J., 2021. Molecular insights into deuterostome evolution from hemichordate developmental
1346 biology. Curr Top Dev Biol 141, 75-117.
1347 Lowe, C.J., Tagawa, K., Humphreys, T., Kirschner, M., Gerhart, J., 2004. Hemichordate embryos:
1348 procurement, culture, and basic methods. Methods Cell Biol 74, 171-194.
1349 Lowe, C.J., Terasaki, M., Wu, M., Freeman, R.M., Jr., Runft, L., Kwan, K., Haigo, S., Aronowicz, J.,
1350 Lander, E., Gruber, C., Smith, M., Kirschner, M., Gerhart, J., 2006. Dorsoventral patterning in
1351 hemichordates: insights into early chordate evolution. PLoS Biol 4, e291.
1352 Lowe, C.J., Wu, M., Salic, A., Evans, L., Lander, E., Stange-Thomann, N., Gruber, C.E., Gerhart, J.,
1353 Kirschner, M., 2003. Anteroposterior patterning in hemichordates and the origins of the chordate nervous
1354 system. Cell 113, 853-865.
1355 Luo, L., 2020. Principles of neurobiology, Second edition. ed. Garland Science, Boca Raton.
1356 Luttrell, S., Konikoff, C., Byrne, A., Bengtsson, B., Swalla, B.J., 2012. Ptychoderid hemichordate
1357 neurulation without a notochord. Integrative and comparative biology 52, 829-834.
1358 Martin-Duran, J.M., Pang, K., Borve, A., Le, H.S., Furu, A., Cannon, J.T., Jondelius, U., Hejnol, A.,
1359 2018. Convergent evolution of bilaterian nerve cords. Nature 553, 45-50.

McIntire, S.L., Jorgensen, E., Kaplan, J., Horvitz, H.R., 1993. The GABAergic nervous system of Caenorhabditis elegans. Nature 364, 337-341.
Metschnikoff, V.E., 1881. Über die systematische Stellung von Balanoglossus. Zool Anz 4, 139-157.
Miller, M.W., 2019. GABA as a Neurotransmitter in Gastropod Molluscs. Biol Bull 236, 144-156.
Minor, P.J., Clarke, D.N., Andrade Lopez, J.M., Fritzenwanker, J.H., Gray, J., Lowe, C.J., 2019. I-SceI Meganuclease-mediated transgenesis in the acorn worm, Saccoglossus kowalevskii. Dev Biol 445, 8-15.
Mirabeau, O., Joly, J.S., 2013. Molecular evolution of peptidergic signaling systems in bilaterians. Proc Natl Acad Sci U S A 110, E2028-2037.
Miyamoto, N., Nakajima, Y., Wada, H., Saito, Y., 2010. Development of the nervous system in the acorn worm Balanoglossus simodensis: insights into nervous system evolution. Evolution & development 12, 416-424.
Miyamoto, N., Wada, H., 2013. Hemichordate neurulation and the origin of the neural tube. Nature communications 4, 2713.
Morgan, T., 1894. Development of Balanoglossus. Journal of Morphology 9, 1-86.
Mueller, T., Vernier, P., Wullimann, M.F., 2006. A phylotypic stage in vertebrate brain development: GABA cell patterns in zebrafish compared with mouse. J Comp Neurol 494, 620-634.
Nakajima, Y., Humphreys, T., Kaneko, H., Tagawa, K., 2004a. Development and neural organization of the tornaria larva of the Hawaiian hemichordate, Ptychodera flava. Zoolog Sci 21, 69-78.
Nakajima, Y., Kaneko, H., Murray, G., Burke, R.D., 2004b. Divergent patterns of neural development in larval echinoids and asteroids. Evolution & development 6, 95-104.
Nicholson, C., 2000. Volume transmission in the year 2000. Prog Brain Res 125, 437-446.
Nieuwenhuys, R., 2000. Comparative aspects of volume transmission, with sidelight on other forms of intercellular communication. Prog Brain Res 125, 49-126.
Nistri, A., Constanti, A., 1979. Pharmacological characterization of different types of GABA and glutamate receptors in vertebrates and invertebrates. Prog Neurobiol 13, 117-235.
Nomaksteinsky, M., Rottinger, E., Dufour, H.D., Chettouh, Z., Lowe, C.J., Martindale, M.Q., Brunet, J.F., 2009. Centralization of the deuterostome nervous system predates chordates. Curr Biol 19, 1264-1269.
Nørrevang, A., 1965. Fine structure of nervous layer, basement membrane, and muscles of the proboscis in Harrimania kupfferi (Enteropneusta). Vidensk. Medd. fra Dansk naturh. Foren. 128, 325-337.
Pani, A.M., Mullarkey, E.E., Aronowicz, J., Assimacopoulos, S., Grove, E.A., Lowe, C.J., 2012. Ancient deuterostome origins of vertebrate brain signalling centres. Nature 483, 289-294.
Parker, H.J., Bronner, M.E., Krumlauf, R., 2014. A Hox regulatory network of hindbrain segmentation is conserved to the base of vertebrates. Nature 514, 490-493.
Pennuto, M., Bonanomi, D., Benfenati, F., Valtorta, F., 2003. Synaptophysin I controls the targeting of VAMP2/synaptobrevin II to synaptic vesicles. Mol Biol Cell 14, 4909-4919.
Pham, K., Hobert, O., 2019. Unlike Drosophila elav, the C. elegans elav orthologue exc-7 is not panneuronally expressed. MicroPubl Biol 2019.
Roberts, E., Chase, T.N., Tower, D.B., City of Hope National Medical Center (U.S.), National Institute of Neurological and Communicative Disorders and Stroke., Kroc Foundation., 1976. GABA in nervous system function. Raven Press, New York.
Roberts, E., Kuriyama, K., 1968. Biochemical-physiological correlations in studies of the gamma-aminobutyric acid system. Brain Res 8, 1-35.
Robinow, S., Campos, A.R., Yao, K.M., White, K., 1988. The elav gene product of Drosophila, required in neurons, has three RNP consensus motifs. Science 242, 1570-1572.
Robinow, S., White, K., 1988. The locus elav of Drosophila melanogaster is expressed in neurons at all developmental stages. Dev Biol 126, 294-303.
Rouille, Y., Duguay, S.J., Lund, K., Furuta, M., Gong, Q., Lipkind, G., Oliva, A.A., Jr., Chan, S.J., Steiner, D.F., 1995. Proteolytic processing mechanisms in the biosynthesis of neuroendocrine peptides: the subtilisin-like proprotein convertases. Front Neuroendocrinol 16, 322-361.

Sanfilippo, P., Smibert, P., Duan, H., Lai, E.C., 2016. Neural specificity of the RNA-binding protein Elav is achieved by post-transcriptional repression in non-neural tissues. Development 143, 4474-4485.
Sato, A., Bishop, J.D., Holland, P.W., 2008. Developmental biology of pterobranch hemichordates: history and perspectives. Genesis 46, 587-591.
Seidah, N.G., Benjannet, S., Hamelin, J., Mamarbachi, A.M., Basak, A., Marcinkiewicz, J., Mbikay, M., Chretien, M., Marcinkiewicz, M., 1999. The subtilisin/kexin family of precursor convertases. Emphasis on PC1, PC2/7B2, POMC and the novel enzyme SKI-1. Ann N Y Acad Sci 885, 57-74.
Silèn, L., 1950. On the nervous system of Glossibalanus marginatus Meek (Enteropneusta). . Acta Zoologica 31, 149-175
Spengel, J.W., 1877. Ueber den Bau und die Entwickelung des Balanoglossus. Amtl. Ber. 50,vers.d. Naturf. U. Artz, 176-177.
Spengel JW. Neue Betrage zur Kenntniss der Enteropneusten 1. Ptychodera flava. Zool. Jahrb., Abt. f. Anat., Bd. 1903;18:271-326.
Tassia, M.G., Cannon, J.T., Konikoff, C.E., Shenkar, N., Halanych, K.M., Swalla, B.J., 2016. The Global Diversity of Hemichordata. PLoS One 11, e0162564.
Tessmar-Raible, K., Raible, F., Christodoulou, F., Guy, K., Rembold, M., Hausen, H., Arendt, D., 2007. Conserved sensory-neurosecretory cell types in annelid and fish forebrain: insights into hypothalamus evolution. Cell 129, 1389-1400.
Tinoco, A.B., Barreiro-Iglesias, A., Yanez Guerra, L.A., Delroisse, J., Zhang, Y., Gunner, E.F., Zampronio, C.G., Jones, A.M., Egertova, M., Elphick, M.R., 2021. Ancient role of sulfakinin/cholecystokinin-type signalling in inhibitory regulation of feeding processes revealed in an echinoderm. Elife 10.
van den Pol, A.N., 2012. Neuropeptide transmission in brain circuits. Neuron 76, 98-115.
Walker, R.J., Papaioannou, S., Holden-Dye, L., 2009. A review of FMRFamide- and RFamide-like peptides in metazoa. Invert Neurosci 9, 111-153.
Watanabe, T., Taguchi, Y., Shiosaka, S., Tanaka, J., Kubota, H., Terano, Y., Tohyama, M., Wada, H., 1984. Distribution of the histaminergic neuron system in the central nervous system of rats; a fluorescent immunohistochemical analysis with histidine decarboxylase as a marker. Brain Res 295, 13-25.
Wiedenmann, B., Franke, W.W., 1985. Identification and localization of synaptophysin, an integral membrane glycoprotein of Mr 38,000 characteristic of presynaptic vesicles. Cell 41, 1017-1028.
Xie Y, Dorsky RI. Development of the hypothalamus: conservation, modification and innovation. Development. 2017 May 1;144(9):1588-99.
Yao, Y., Minor, P.J., Zhao, Y.T., Jeong, Y., Pani, A.M., King, A.N., Symmons, O., Gan, L., Cardoso, W.V., Spitz, F., Lowe, C.J., Epstein, D.J., 2016. Cis-regulatory architecture of a brain signaling center predates the origin of chordates. Nat Genet 48, 575-580.
Zhang S, Ji X. Hatschek's pit and origin of pituitary gland. Acta Oceanologica Sinica. 2022 Dec;41(12):1-6.
Zhang, X., Pan, H., Peng, B., Steiner, D.F., Pintar, J.E., Fricker, L.D., 2010. Neuropeptidomic analysis establishes a major role for prohormone convertase-2 in neuropeptide biosynthesis. J Neurochem 112, 1168-1179.
Zoeller RT, Tan SW, Tyl RW. General background on the hypothalamic-pituitary-thyroid (HPT) axis. Critical reviews in toxicology. 2007 Jan 1;37(1-2):11-53.

Figure 1: Pan-neural marker, ELAV, expression

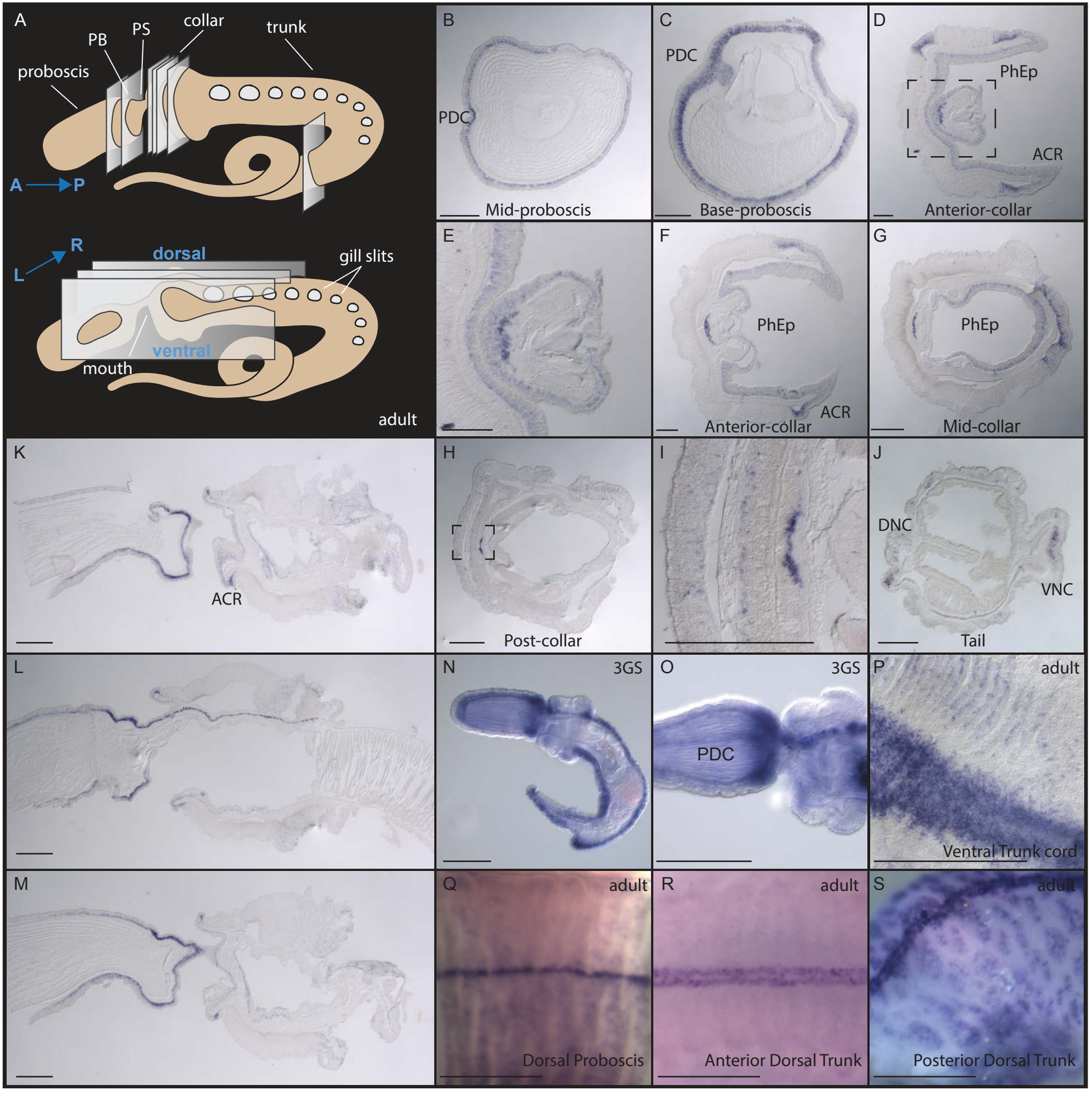

Figure 2: Expression of neurotransmitter markers

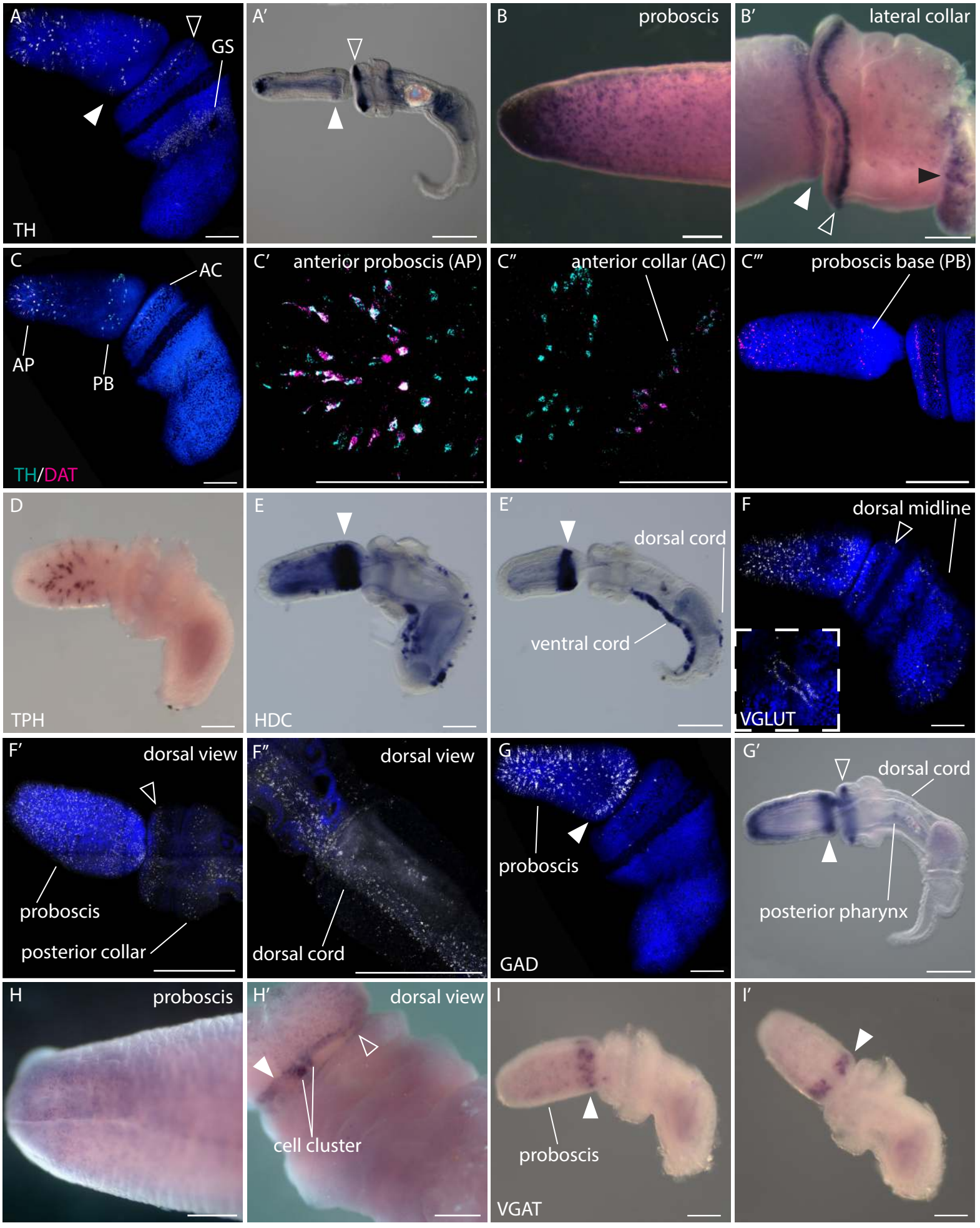

Figure 3: Expression of neuropeptide markers

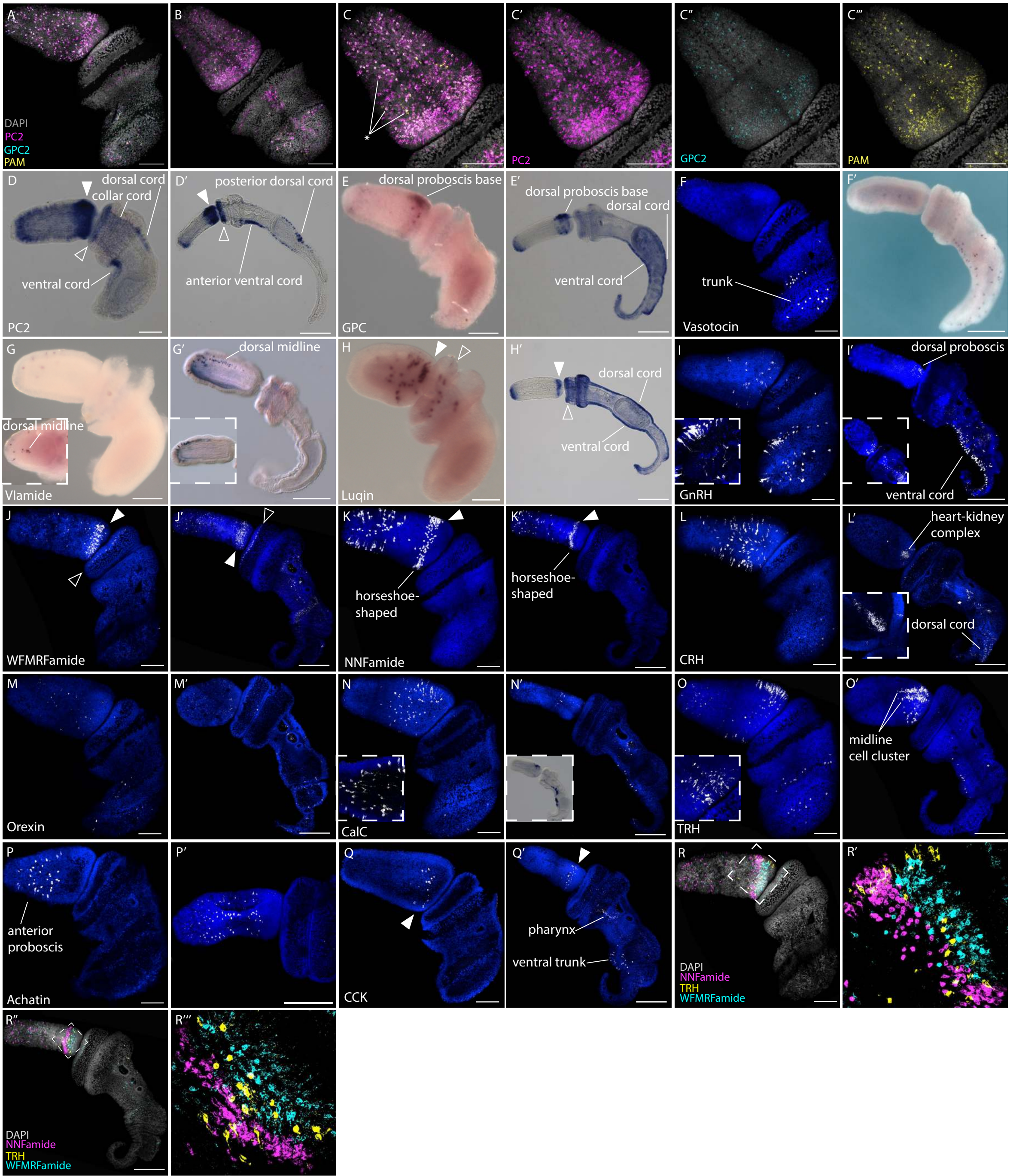

Figure 4: Neural plexus organization

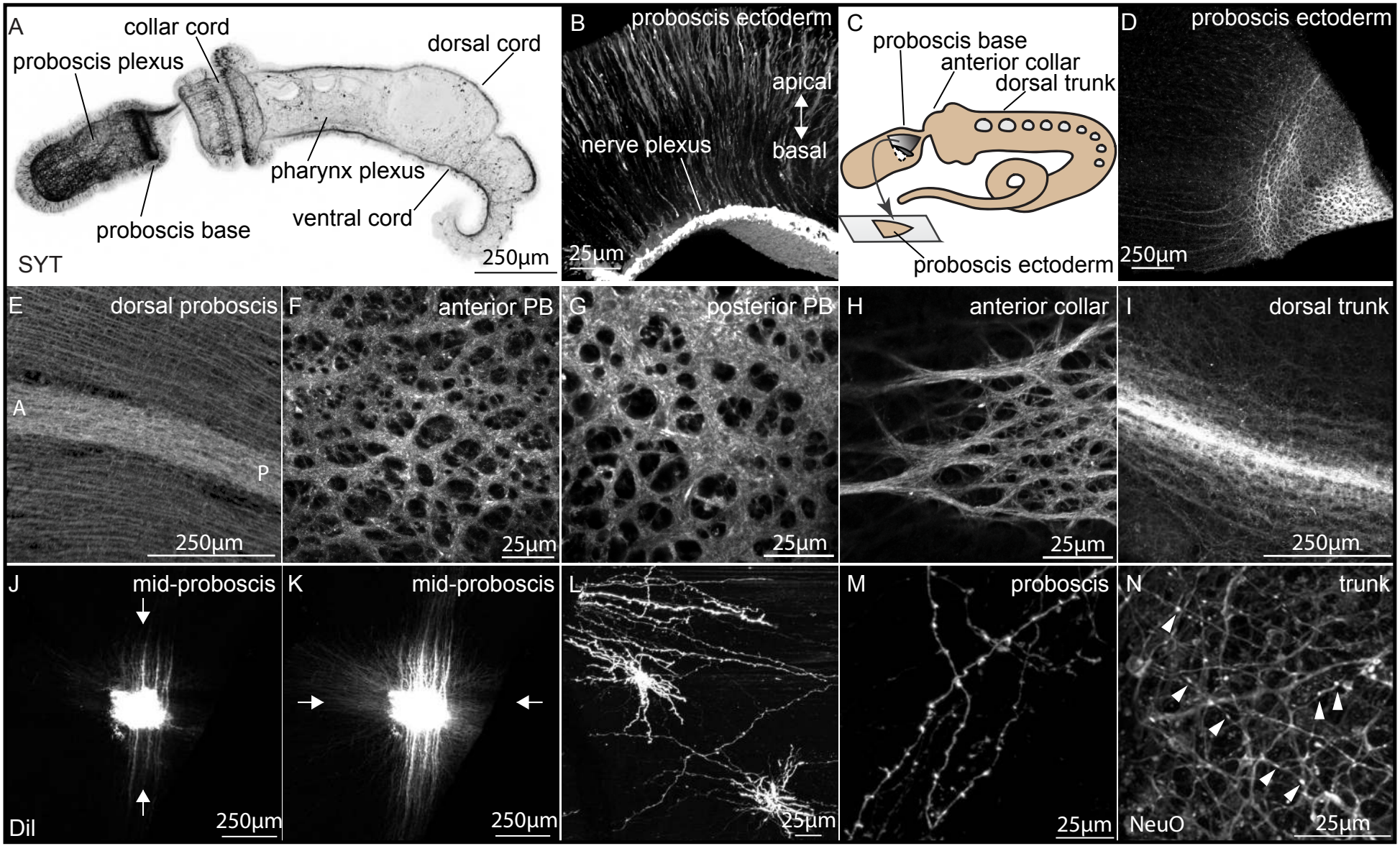

Figure 5: Serotonergic nervous system

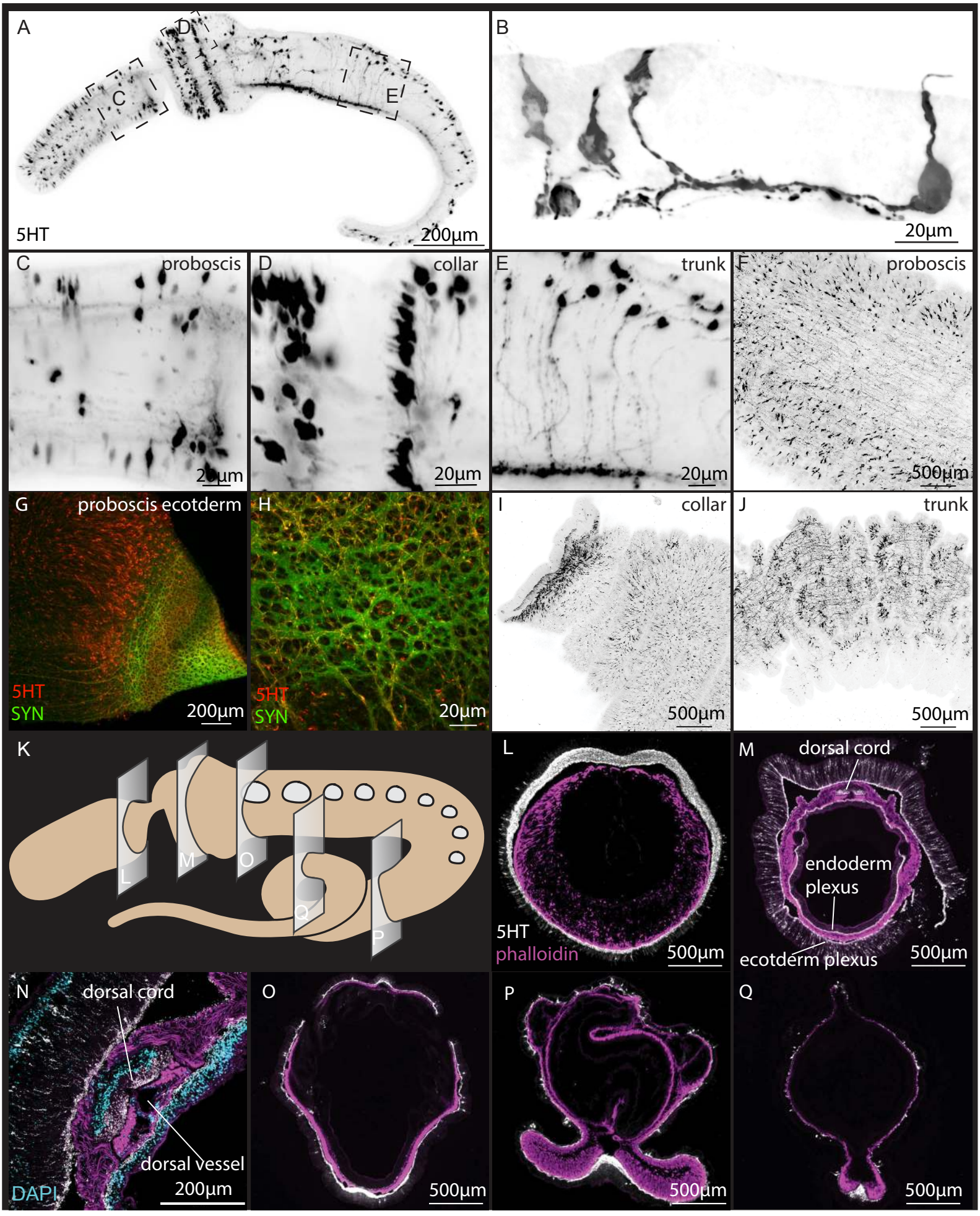

Figure 6: GABAergic and FMRFamidergic nervous system

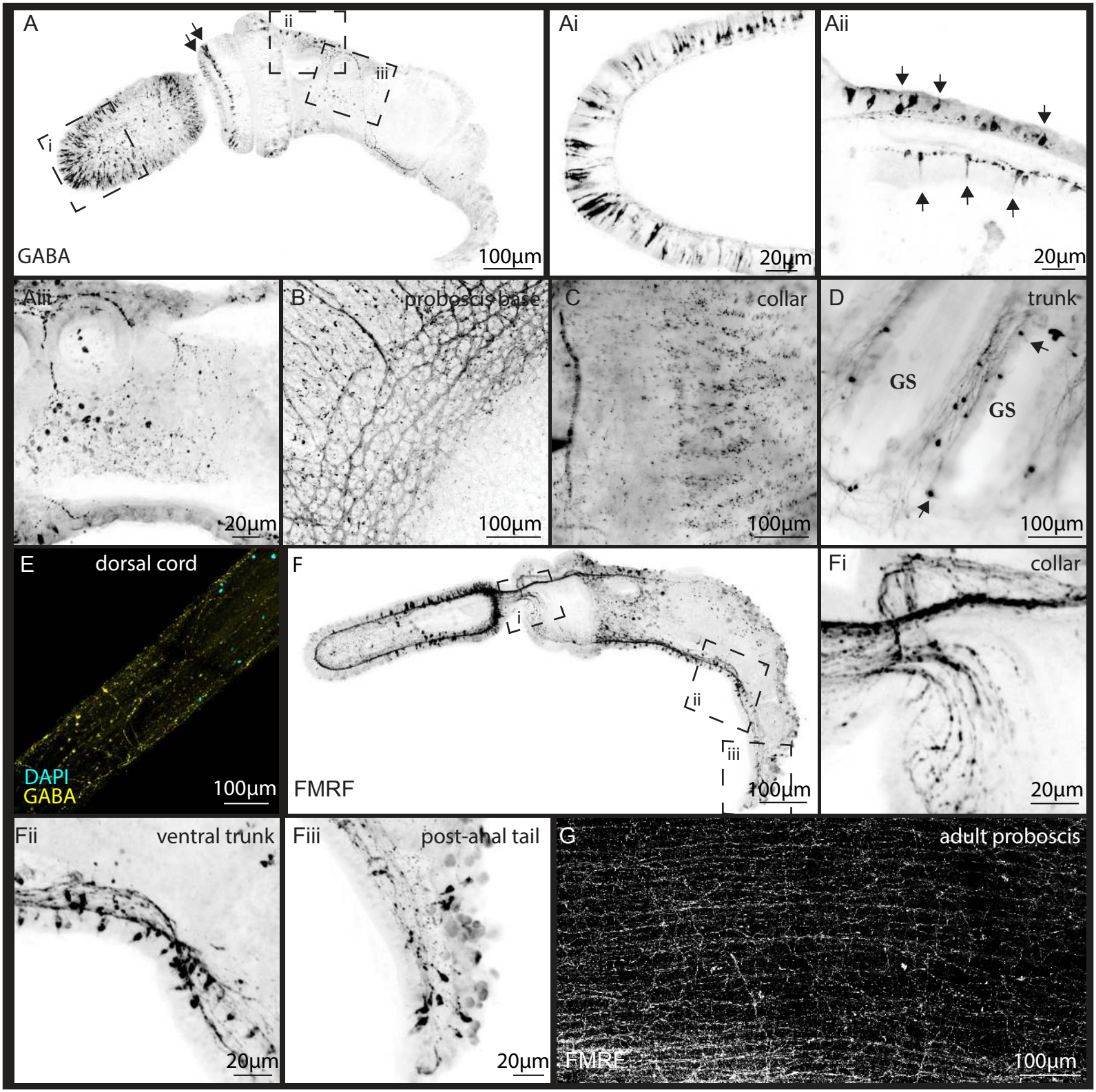

Figure 7: Neural cell morphology and neurite projection using a synapsin:GFP transgene

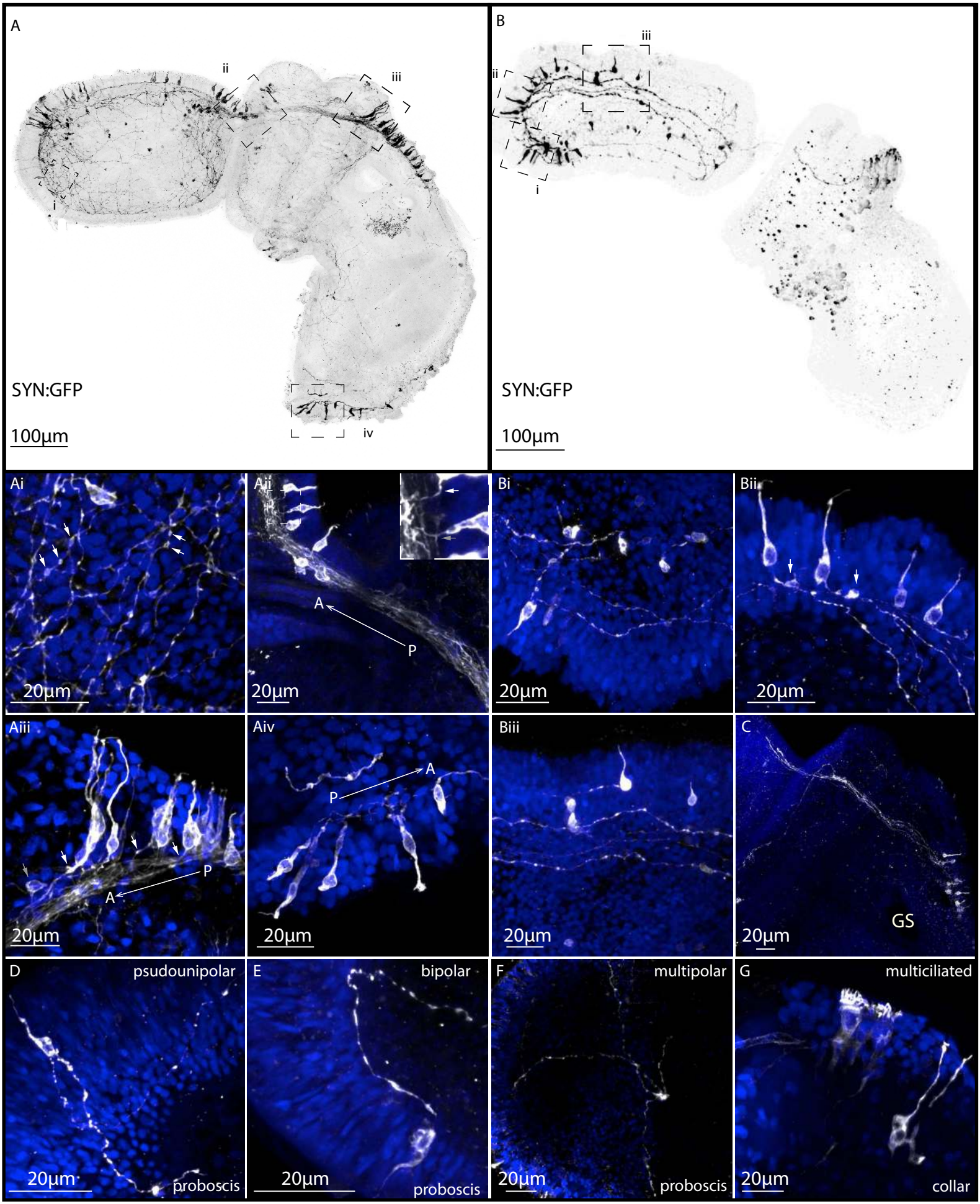

Figure 8: Localization of synaptophysin along axons at varicosities

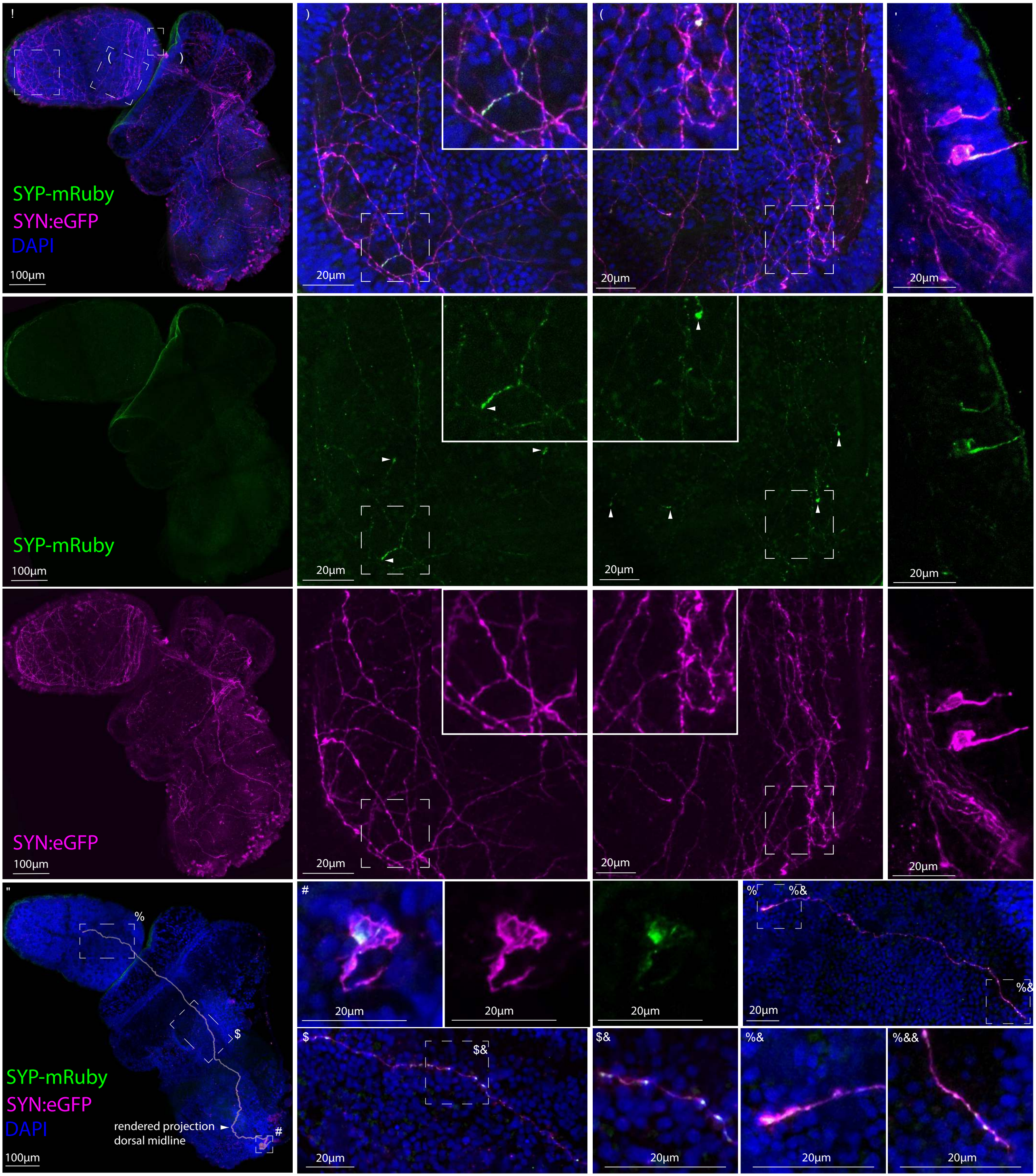
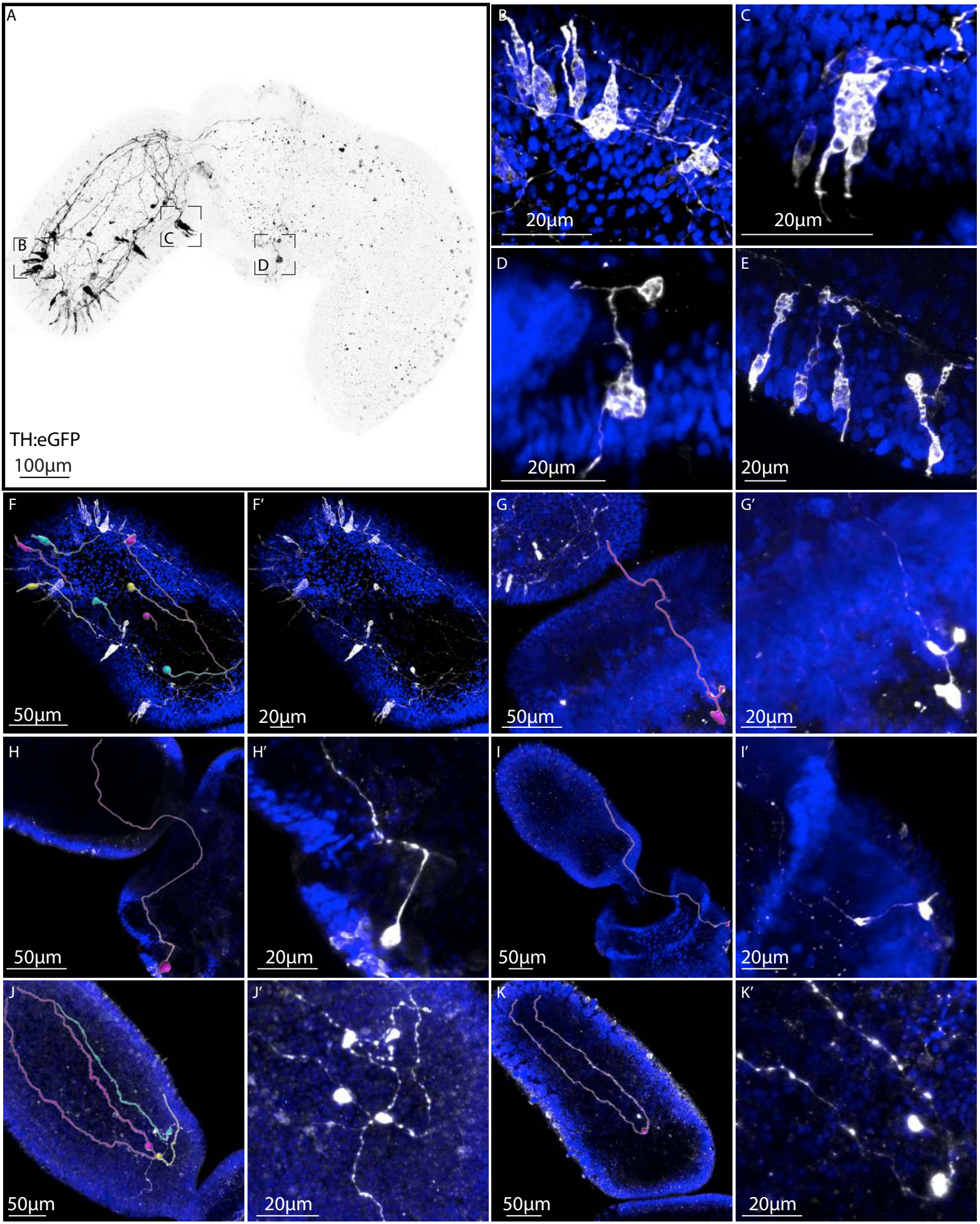
Figure 9: TH:GFP transgene